Nanoscale Advances

ROYAL SOCIETY OF CHEMISTRY

PAPER

View Article Online
View Journal | View Issue

Cite this: *Nanoscale Adv.*, 2025, **7**, 7705

Pumpkin-waste-derived copper quantum dots: green synthesis, underlying mechanism, and multifunctional applications in catalysis, antioxidants, and bioimaging

Lamis Dayoub, *[a] Xiaoxuan Li,[a] Xuewen Peng,[a] Wajeeha Pervaiz,[a] Shoulei Yan[a] and Yiping Chen *[ab]

Agricultural waste poses a significant challenge and opportunity for sustainable nanotechnology. This study presents a novel, eco-friendly, and cost-effective green synthesis of copper quantum dots (CuQDs) utilizing pumpkin waste extract. Our mechanistic investigations using LC-MS revealed a three-phase process (reduction, nucleation, and stabilization) driven by synergistic phytochemical interactions, providing key insights into CuQDs formation. The synthesized CuQDs exhibit rich optical properties, including strong fluorescence emission and a narrow size distribution (4 ± 0.4 nm). These CuQDs demonstrated significant catalytic efficiency, achieving 90% degradation of crystal violet and 96% of methylene blue within 3 min, alongside notable antioxidant activity. These functionalities are directly correlated with the elucidated mechanistic insights, where phytochemicals not only facilitate synthesis but also impart inherent bioactivity. Furthermore, CuQDs exhibited robust tissue-specific accumulation and bright fluorescence in zebrafish embryos, highlighting their potential for real-time bioimaging. Biocompatibility assessments confirmed minimal toxicity, with normal embryonic development and hatching rates, and environmental safety was validated through seed germination experiments. This green synthesis method offers a superior, sustainable alternative to conventional approaches by eliminating toxic chemicals and energy-intensive processes, thereby advancing environmentally responsible nanomaterial production.

Received 21st August 2025
Accepted 5th October 2025

DOI: 10.1039/d5na00813a

rsc.li/nanoscale-advances

1. Introduction

The management of agricultural waste has become a pressing global concern due to the increasing volume of by-products generated from food production and processing. These wastes, often rich in bioactive compounds such as polyphenols, proteins, unsaturated fatty acids, minerals, and vitamins, represent an underutilized resource with immense potential for sustainable applications in nanotechnology and environmental remediation.[1,2] For instance, pumpkin waste, with its abundance of bioactive compounds, acts as an effective reducing, capping, and stabilizing agent in the synthesis of functional nanomaterials.[3,4] In this context, the development of green synthesis methods using agricultural waste has emerged as a promising strategy to address both waste management and resource recovery challenges.

Quantum dots (QDs) have gained significant attention due to their unique properties, such as ultra-small size (2–10 nm), tunable fluorescence, and quantum confinement effects, which enable precise control over their electronic and optical behaviors. Unlike conventional nanoparticles (NPs), QDs exhibit superior luminescence properties, including narrow emission spectra, high photostability, and wide absorption spectra, making them ideal for applications in catalysis, biomedicine, and environmental remediation.[5,6] Furthermore, their large surface-to-volume ratio enhances their efficiency in antioxidant and catalytic applications, surpassing the capabilities of traditional NPs.[7] Copper, in particular, is an attractive material for QDs synthesis due to its cost-effectiveness, natural abundance, and excellent catalytic/antioxidant properties, aligning with the goals of sustainable nanotechnology. Its recognition as generally recognized as safe (GRAS) and its biocompatibility further support its use in applications such as active packaging and contaminant degradation, ensuring minimal toxicity and regulatory compliance.[8]

Unlike conventional synthesis methods, which often rely on toxic chemicals, high energy consumption, and complex procedures, green synthesis approaches utilizing plant-based extracts offer a sustainable, cost-effective, and eco-friendly alternative.[9,10] In the field of bioimaging, QDs have become indispensable due to their tunable fluorescence, photostability,

[a]College of Food Science and Technology, Huazhong Agricultural University, Wuhan 430070, Hubei, China. E-mail: mmn87@yahoo.com
[b]State Key Laboratory of Marine Food Processing and Safety Control, Dalian Polytechnic University, Dalian, Liaoning, 116034, China. E-mail: chenyiping@hzau.edu.cn

and biocompatibility, enabling real-time, high-resolution visualization of cellular and molecular processes. However, the toxicity and environmental impact of conventional QDs, such as those based on cadmium, have limited their widespread use. CuQDs, with their low toxicity and excellent optical properties, present a compelling alternative for bioimaging applications.[11]

Earlier plant-based QDs had narrow scope. One study used a root extract to make CuQDs around 22.68 nm wide and tested only antibacterial effects.[12] Another article used a one-pot hydrothermal method to make carbon quantum dots (CQDs) from waste shells and noted tunable fluorescence and good biocompatibility for bioimaging.[13] In contrast, our work uses pumpkin waste and reveals the formation mechanism. LC-MS showed a three stages mechanism including reduction, nucleation and stabilization, driven by phenolic acids, flavonoids and nitrogen compounds. CuQDs are about 4 nm across and emit bright fluorescence. They degrade crystal violet (CV) and methylene blue (MB) quickly, scavenge free radicals, and produce clear, multi-color images in zebrafish embryos without toxicity. By explaining the mechanism and demonstrating multi-dye degradation, antioxidant activity and *in vivo* imaging, this study shows that waste-derived CuQDs can be versatile nanomaterials rather than single-use agents.

2. Materials and methods

2.1 Reagents/materials

Fresh giant pumpkins (*Cucurbita moschata*) were obtained from Huazhong Agriculture University supermarket, Main Campus, Wuhan, China. Copper sulfate pentahydrate ($CuSO_4 \cdot 5H_2O$, 99.99%) was purchased from Sigma-Aldrich. Ascorbic acid was procured by SCR Co., Ltd (China). LLC. MB was purchased from Tianxin Chemical Co., Ltd, Tianjin, China, while CV was obtained from Biosharp-China. NaOH, HCl, and 1,1-diphenyl-2-picrylhydrazyl (DPPH) were sourced from Shanghai Macklin Biochemical Chemical Co. Ltd (Shanghai, China). Methanol and ethanol were purchased from SCR Co., Ltd (China). Zebrafish embryos (*Danio rerio*) of the AB strain were obtained from (Zebrafish Research Service Center, Wuhan, China) and maintained in compliance with institutional ethical guidelines for animal care. The Hank's solution was purchase from Shanghai Fisher Biotechnology Co (China). All chemicals and materials used in this study were of analytical grade. Ultrapure water was obtained from (Milli-Q Plus, Millipore Inc., Bedford, MA, USA). All chemicals were used directly without further purification. Clean and oven-dried glassware was used in the synthesis of CuQDs. All solvents used for LC-MS analysis were of LC-MS grade (Sigma-Aldrich, Germany).

2.2 Green synthesis of CuQDs

Fresh pumpkin was thoroughly washed several times with distilled water. To prepare the pumpkin waste extract, the peels were removed, cut into 1–2 cm^2 pieces, and dried under a fan for two days. The peels were then minced into powder. Ten grams of the obtained peels powder with 50 g of seeds and pulp were minced using a mixer, added to 500 mL of ultrapure water, and heated in a water bath at 60 °C under a magnetic stirrer at 650 rpm for 120 min. The extract was filtered through Whatman No. 1 filter paper (11 μm pore size), and the filtrate was stored at 4 °C. The resulting filtrate solution 50 mL was then treated with an aqueous solution of freshly prepared 1 mL of 0.1 M copper sulfate in a water bath at 50 °C a magnetic stirrer at 650 rpm. Qualitatively, the synthesis of the CuQDs was verified by observing the color transformation of the solution from orange to light brown with constant stirring at 50 °C. Next the resultant solution was centrifuged at 8000 rpm for 10 min and the supernatant was collected.

Prior to employing the protocols for synthesis and applications, an optimization procedure was conducted to determine the most effective parameters for the green synthesis of CuQDs. The optimization focused on key variables, including the quantity of pumpkin waste extract, copper sulfate concentration, pH, incubation temperature, and reaction time, as these factors influence the size, stability, and functionality of the synthesized CuQDs. Various amounts of pumpkin waste extract were tested to determine the optimal concentration for efficient reduction and capping of copper ions. Different concentrations of copper sulfate were also evaluated, with the most effective concentration. The pH ranges from 4 to 8 was studied, to find the most suitable pH value for facilitating the reduction of Cu^{2+} ions while maintaining the stability of the CuQDs. Temperature tests were carried out between 40–80 °C. The reaction time was varied between 1 and 3 hours to find the best results in terms of the reduction of copper ions and achieving high-quality CuQDs with narrow size distribution.

2.3 Characterization of CuQDs

The optical properties of the CuQDs were analyzed using a UV-visible spectrophotometer (Genesys 150, Thermo Scientific, USA) in the range of 200–800 nm. Fluorescence spectra were recorded using an F-4600 fluorescence spectrophotometer (Hitachi, Tokyo, Japan) at an excitation wavelength of 380 nm, with additional measurements taken across excitation wavelengths of 300–480 nm.

Fourier Transform Infrared (FTIR) spectroscopy (Thermo Scientific Nicolet iS50 spectrometer) was employed to identify functional groups in the pumpkin waste extract and CuQDs, with spectra recorded in the range of 400–4000 cm^{-1}. The morphology and particle size of the CuQDs were examined using transmission electron microscopy (TEM, JEOL 3010 UHR, operating at 100 kV). High-resolution images and selected area electron diffraction (SAED) patterns were obtained using a JEM-2100 microscope (JEOL, Japan) at an accelerating voltage of 200 kV. The stability of the CuQDs was assessed by measuring their zeta potential. Surface composition and structural analysis were performed using X-ray photoelectron spectroscopy (XPS, VG ESCALAB 220i-XL).

The quantum yield (QY) of the sample was determined using rhodamine in ethanol as a standard. Spectroscopic data for the sample and the standard were collected, and the integrated area under the emission spectrum was computed using numerical integration. The QY was calculated as: $\Phi = \Phi_{st} \times (I/I_{st}) \times (\eta/\eta_{st})$.[2]

Where: Φ = QY of the sample, Φ_{st} = QY of the standard, I = integrated intensity of the sample, I_{st} = integrated intensity of the standard, η = refractive index of the sample. η_{st} = Refractive index of the standard, where QY of the standard is 0.95 for rhodamine.

2.4 Catalytic activity for dye degradation of CuQDs

The catalytic activity of the CuQDs was evaluated by studying their catalytic effect on the degradation of organic dyes, specifically MB and CV. For each dye, 30 mL of 100 mg L^{-1} MB and 30 mL of 100 mg L^{-1} CV were separately prepared in 100 mL conical flasks. A mixture containing 30 mL of MB and 30 mL of CV (1 : 1 ratio) was also prepared for further evaluation of CuQDs' ability to degrade a mixture of these two dyes. To begin the reaction, 1 mL of the synthesized CuQDs solution (100 μg mL^{-1}) was added to each dye solution, followed by hand shaking to ensure proper mixing. The control experiments were conducted using only the dye solutions without CuQDs.

The degradation process of MB and CV was studied over a pH range of 3–11, which was adjusted using 0.01 M NaOH and HCl solutions. The treated dye solutions were monitored for their absorbance at 200–700 nm using a UV-Vis spectrophotometer, and the absorbance measurements were taken every 15 min. The degradation efficiency was quantified by calculating the degradation ratio using the formula: Ratio of degradation = $(A_0 - A_t)/A_0$. Where A_0 is the initial absorbance and A_t is the final absorbance.

2.5 Enhancement of catalytic effect by addition of $NaBH_4$

The catalytic effect of CuQDs on dye degradation was enhanced by the addition of sodium borohydride ($NaBH_4$). To each dye solution (30 mL of MB or CV at 100 mg L^{-1}), 0.5 mL of 0.5 mg mL^{-1} $NaBH_4$ was added to facilitate the reduction process. Afterward, 1 mL of the synthesized CuQDs solution (100 μg mL^{-1}) was introduced to the mixture, and the solution was shaken to ensure uniform distribution of the CuQDs and $NaBH_4$.

The same testing procedure as described in the catalytic activity experiment was followed, with the UV-Vis spectrophotometer measuring the absorbance at 200–700 nm every 15 min. The degradation efficiency was again calculated using the formula for degradation ratio, allowing a direct comparison of the catalytic effect with and without $NaBH_4$. The results from these experiments help highlight the enhanced catalytic activity when $NaBH_4$ is used in conjunction with CuQDs.

2.6 Antioxidant activity of CuQDs

The antioxidant properties of the CuQDs were evaluated using freshly prepared DPPH as a free-radical model, as described previously.[7] Various concentrations (10, 30, 50, 70, and 100 μg mL^{-1}) of pumpkin waste extract and CuQDs were added to 2000 μL of 0.1 mM DPPH solution in absolute methanol with the addition of distilled water to make a final volume of 3000 μL. The resultant reaction mixtures were shaken vigorously and incubated for 30 min at 37 °C in the dark. The control was prepared by adding 1000 μL distilled water to 2000 μL DPPH solution, and ascorbic acid was used as a positive control. The transformation of color from violet to yellow was detected because of its antioxidant potential. The UV-Vis spectrum of the reaction mixture was recorded at 517 nm.

The inhibition percentage of antioxidant activity was calculated using the equation: Scavenging activity (%) = $(A_0 - A_1/A_0) \times 100$. Here, A_0 is the absorbance of the DPPH radical and A_1 is the absorbance of the test sample. The tested samples included CuQDs, pumpkin extract, and ascorbic acid.

2.7 Seed germination assessment of CuQDs

The effect of CuQDs on seed germination was examined using green gram seeds that had been soaked overnight in CuQDs solution using the following ratios of CuQDs (10, 30, 50, 80, and 100%) and control in distilled water (without CuQDs). The seeds were sterilized with 1 mL of 100% ethanol before the experiment and then submerged in a solution of 3% sodium hypochlorite for 15 min on Whatman filter paper in a Petri dish, with a 1 cm distance between each seed.[11] The Petri dishes were placed in the dark in a growth chamber at 25 °C. The plates were imaged after incubation for seven days at room temperature. And growth was measured using a millimeter ruler. The seed germination experiment was repeated three times under identical conditions to ensure reproducibility. The data presented in the manuscript represent the average values obtained from these three independent trials, confirming the reliability and consistency of the observed results.

2.8 Bioimaging and toxicity

Fluorescence analysis, a cornerstone of bioanalysis, offers high sensitivity for detecting and tracking biomolecules in complex biological systems.[14] Zebrafish (*Danio rerio*) are commonly used model as *in vivo* model systems in the toxicity studies of nanomaterials. The transparency of the zebrafish body during the early stages of embryonic development makes it easy to monitor *in vivo* transmission, biocompatibility, toxicity, and fluorescence probes of various NPs.[15] Wild-type AB strain zebrafish embryos and larvae were used as *in vivo* models for toxicity and imaging studies. Fertilized zebrafish embryos were collected within 1.5 hours post-fertilization (hpf) and cultured in Hank's solution at 28 °C under a 14 : 10 light–dark cycle. Larvae were maintained in standard laboratory conditions. CuQDs were introduced to zebrafish eggs *via* soaking embryos in CuQDs solution. Animal experiment was conducted in strict accordance with the animal welfare guidelines of the World Organization for Animal Health. All procedures were performed following the Guidelines for the Care and Use of Laboratory Animals of Huazhong Agricultural University (Wuhan, China) and were approved by the Hubei Provincial Animal Care and Use Committee.

Sixty marked Zebrafish eggs were exposed to CuQDs at varying concentrations (0, 20, 40, 60, 80, and 100 μg mL^{-1}) dispersed in Hank's solution. Groups of 10 embryos per concentration were cultured in 24-well plates and incubated for up to 120 hours. The embryos were moved to respective wells for the development of the eyes, tail, and head. For larval imaging

studies, 5 days post-fertilization (dpf) larvae were soaked in 100 μg mL^{-1} CuQDs solution for 12 hours, followed by washing thrice with Hank's solution to remove excess particles. Fluorescence imaging was conducted to assess the *in vivo* distribution and bioimaging potential of CuQDs. Imaging was performed using an inverted fluorescence microscope (Nikon Eclipse Ti-S, Japan). The system was equipped with UV (EX 330–380 nm, DM 400 nm, BA 410 nm), green (EX 465–495 nm, DM 505 nm, BA 515–555 nm), and red (EX 540–580 nm, DM 595 nm, BA 600–660 nm) filter cubes. Observations were made at 24, 48, 96, and 120 hpf. Magnifications of 10× and 20× were employed to capture detailed images of tissue distribution. Fluorescence intensity and tissue distribution patterns were analyzed using imaging software. Moreover, the survival and hatching rates were measured each 24 h time duration to excrete impurity on the suspension.

2.9 Underlying mechanism of CuQDs green synthesis

Pumpkin extract and CuQDs samples were filtered through syringe filters (PTFE 13 mm, 0.22 μm discs, Kinesis KX, Vernon Hills, USA) into 2 mL glass vials (Agilent Technologies, Santa Clara, USA). Samples were analyzed: (1) pumpkin waste extract and (2) CuQDs synthesized from pumpkin waste extract. LC-MS analysis was performed using an Agilent 1290II UHPLC system (Agilent, USA) coupled with an Agilent 6460 triple quadrupole mass spectrometer (Agilent, USA) in both negative and positive ionization modes.

Chromatographic separation was performed on an Agilent ZORBAX Eclipse Plus C18 column (2.1 × 100 mm, 1.8 μm) maintained at 40 °C. The mobile phase consisted of (A) 0.1% formic acid in water and (B) 0.1% formic acid in acetonitrile, delivered at a flow rate of 0.3 mL min^{-1}. The gradient elution program was set as follows: 0–1 min, 5% B; 1–10 min, 5–95% B; 10–12 min, 95% B; 12–12.1 min, 95–5% B; and 12.1–15 min, 5% B for column re-equilibration. The injection volume was 5 μL. Mass spectrometric detection was performed using electrospray ionization (ESI) in both negative and positive ion modes. The scan range was set to *m*/*z* 50–1500. In negative ion mode, the capillary voltage and fragmentor voltage were set to 3500 V and 80 V, respectively. In positive ion mode, the capillary voltage and fragmentor voltage were optimized to 4000 V and 100 V, respectively. The following parameters were common to both modes: nebulizer gas pressure at 45 psi, drying gas flow rate at 10 L min^{-1} (350 °C), and collision energy at 0 V. Peak detection, integration, and alignment were performed using Agilent MassHunter software. Compounds were identified based on retention time, mass spectral data, and literature reports. For comparative analysis, percent change in peak area was calculated as: [(area in sample 2 − area in sample 1)/area in sample 1] × 100.

3. Results and discussion

3.1 Characterization of CuQDs

3.1.1 UV-Vis absorption spectroscopy. UV-Vis has emerged as a valuable tool to characterize and validate the synthesis of QDs in aqueous suspensions. The synthesized CuQDs exhibited a maximum absorption band at 256 nm. As shown in (Fig. 1A), which corresponds to surface plasmon resonance (SPR).

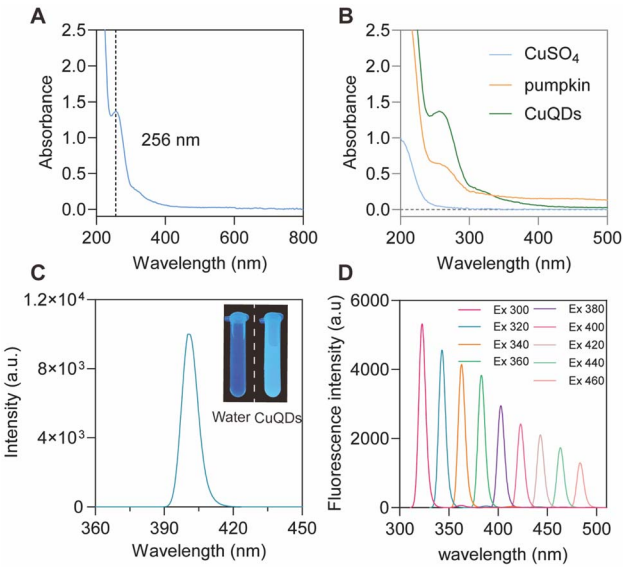

Fig. 1 Physical characterization of the obtained CuQDs. (A) UV-Vis absorption spectrum of CuQDs from 200 to 800 nm, (B) UV-Vis absorption spectrum of $CuSO_4$, pumpkin waste extract, and CuQDs, (C) fluorescence spectra of CuQDs at excitation 380 nm, With images of synthesized CuQDs and control (water) under the UV light, (D) fluorescence spectra of CuQDs at different excitation wavelengths (300–460 nm).

The blue shift in the curve can be explained by nucleation/growth of CuQDs within the 'quantum confinement regime', *i.e.* the absorption band shifted into smaller wavelength compared to the larger copper nanoparticles (Cu NPs) at 560–600 nm.[9,16,17] The strong absorption peak at 256 nm was attributed to the π–π* transition of the aromatic C=C bonds, consistent with the formation of CuQDs.[18] Fig. 1B shows the UV-Vis absorbance of the CuQDs, pumpkin waste, and $CuSo_4$ within the range of 200 to 500 nm.

The optimized conditions were determined to be 50 mL of pumpkin waste extract, 1 mL of 0.1 M copper sulfate, pH 6, and incubation for 2 hours at 50 °C under constant stirring at 650 rpm. These conditions were used in all subsequent experiments to ensure consistency and reproducibility in the synthesis and application of CuQDs. Our optimized green synthesis system offers advantages over conventional methods that usually require harsh chemicals, extreme temperatures, and complex procedures. Green synthesis methods for QDs reduce the environmental impact while maintaining or enhancing the desired optical properties.[19] This is consistent with the growing consensus in the field that plant-mediated QDs synthesis offers a sustainable alternative without compromising the quality and optical properties of the resulting nanomaterials.[20]

3.1.2 Fluorescence analysis. Fluorescence spectroscopy revealed that CuQDs synthesized from pumpkin waste exhibit strong, tunable optical properties. When excited at 380 nm (30

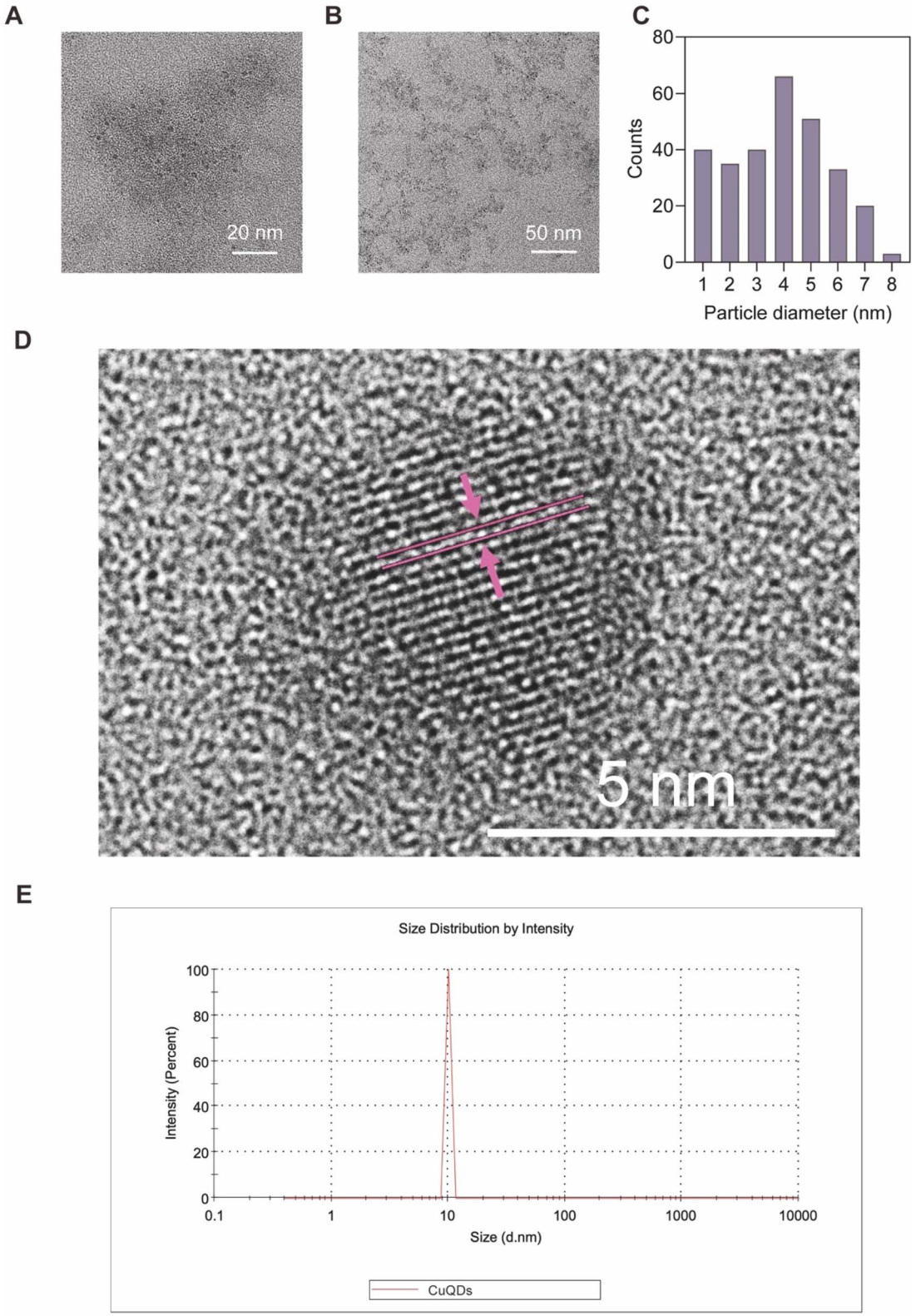

Fig. 2 Physical characterization of the obtained CuQDs: (A and B) Typical TEM images of CuQDs at different magnifications; (C) TEM Size distribution of CuQDs, showing an average size of 4 ± 0.4 nm; (D) HRTEM image of CuQDs, clearly displaying the lattice fringes; (E) size distribution of the CuQDs measured using dynamic light scattering.

μL CuQDs diluted in 10 mL water), the solution displayed characteristic sky-blue fluorescence under 365 nm UV light (Fig. 1C). The emission intensity was concentration-dependent, and red-shifted from 300 to 460 nm as excitation wavelength increased, with a corresponding decrease in intensity (Fig. 1D). The characteristics of the obtained CuQDs were consistent with those of previously described CuQDs.[9,21]

These properties align with the quantum confinement effect, where smaller particle sizes increase band gap energy, leading to excitation-dependent emission. Unlike conventional QDs, these green-synthesized CuQDs require no external passivator; natural organics in the pumpkin waste enhance fluorescence stability and suppress non-radiative recombination. Compared to chemically synthesized QDs, they offer two main advantages: (i) higher QY, stability, and biocompatibility; and (ii) broad-spectrum, excitation-tunable emission (300–500 nm), enabling multicolor bioimaging and multi-target tracking, consistent with findings by Jing *et al.*.[20]

3.1.3 Morphological and size distribution of CuQDs. The morphology and size of the CuQDs samples were determined by TEM. The TEM images of the prepared CuQDs showed spherical shapes of the biosynthesized CuQDs with a homogenous size distribution (Fig. 2A and B). The particle size of the CuQDs was determined using ImageJ software (V.1.54f, National Institutes of Health, Bethesda, Maryland, USA). The results are shown in Fig. 2C. The particle size of the CuQDs was limited to 1–8 nm and the calculated mean size was 4 ± 0.4 nm. Regarding the particle dispersion state and the absence of any agglomeration in the obtained figures, it was confirmed that plant organic surfactants could perform their structure-directing roles effectively. In high-resolution TEM (HRTEM), (small window in Fig. 2D), the observation further suggests that the CuQDs have a graphitic crystalline structure with a lattice spacing of approximately 0.21 nm, which refers to the regular atomic arrangement and distances within the QDs, reflecting their crystal structure and influencing their unique properties. Additionally, we measured the hydrodynamic size of CuQDs in water by DLS. The intensity distribution showed a single, narrow peak centered at 10.10 nm (Fig. 2E). Reported sizes are intensity weighted. This value is larger than the TEM core size of 4 ± 0.4 nm, which reflects the ligand shell and hydration layer around the particles in solution. The distribution showed no secondary peaks above 100 nm, indicating minimal aggregation during measurement.

TEM analysis of pumpkin waste-derived CuQDs revealed uniformly spherical NPs with a narrow size distribution (1–8 nm) and an optimal mean size of 4 ± 0.4 nm, ideal for quantum confinement effects and biological applications.[19] HRTEM analysis confirmed a crystalline, graphitic structure with a lattice spacing of 0.21 nm, indicating high-quality QDs with superior optical properties and stability compared to amorphous counterparts. Such crystallinity is critical for enhanced QY and photostability.[22] The small, uniform size of these CuQDs (<10 nm) facilitates effective biological interactions, improved cellular uptake, and reduced cytotoxicity.[23]

The QY was calculated as QY = 22.99%. This indicates a relatively moderate fluorescence emission efficiency, which suggests a stable and reasonable QY suitable for certain fluorescence applications. To contextualize this finding, we compared our QY with values reported in the literature for both green and chemically synthesized copper-based quantum dots. One study reported green-synthesized near-infrared copper-doped carbon dots (Cu-dCDs) with a fluorescence QY of 11.1%.[24] This suggests that our CuQDs exhibit a significantly higher QY compared to some green-synthesized carbon-based systems. That used oyster shells through a hydrothermal synthesis method, showed a QY value of 1.4% and the QDs from palm showed QY value of 2.4%, while the addition of citric acid resulted in a QY value of 22.1%.[13] For chemically synthesized systems, Cu : InP/ZnSe/ZnS multishell QDs have been reported to achieve a photoluminescence QY of 70%.[25] This highlights the potential for very high QY values in more complex, engineered QDs structures.

3.1.4 FTIR spectroscopy. FTIR analysis was performed for both green-synthesized CuQDs and pumpkin waste extract to identify functional molecules, as the pumpkin waste extract possesses functional groups that assist in the CuQDs synthesis process. FTIR spectra of aqueous extract of pumpkin waste and green synthesized CuQDs presented a wide absorption band which shifted from 3277 to 3293 cm^{-1}. This can be attributed to the hydrogen-bonded O–H groups of alcohols and phenols, as well as the presence of amines or N–H amide in the pumpkin extract, which can be attributed to the capping and stabilization of the QDs.[26] The peak at 2925 cm^{-1} indicates the C–H stretching vibration of phenolic and flavonoid compounds, suggesting their role in reducing copper (Cu) ions and stabilizing CuQDs.[27] CuQDs exhibited a narrow sharp peak around 1623 cm^{-1}, corresponding to the C=O/N–H assignment amide and amine, indicating the presence of amide linkages essential for CuQDs stability.[3] The band at 1532 cm^{-1} that disappeared in the QDs corresponds to the C=C stretch in aromatic rings that are responsible for the capping and stabilization of CuQDs. Moreover, the peaks at 1369 cm^{-1} and 1240 cm^{-1} correspond to O–H and C–H, respectively, which refer to polyphenols, and confirm the aromatic group that offers stability.[26,28]

The peaks at 1021 and 1010 cm^{-1} are assigned to C–O–C and secondary –OH of phenolic groups. They may also correspond to carbonyl stretch vibrations in amide linkages of proteins. The carbonyl group from amino acid residues and peptides shows strong binding with copper.[28] The bands at 604 and 580 cm^{-1} correspond to C–H bonds, indicating alkanes and flavonoids.[26,28] However, the observed band at 1123.36 cm^{-1}, which was not present in the pumpkin waste extract sample, corresponded to the obtained CuQDs[7] (Fig. 3). Table 1 presents the FTIR spectra of the pumpkin waste and CuQDs, corresponding to their functional groups.

FTIR analysis of both the green-synthesized CuQDs and pumpkin waste extract revealed essential information about the functional groups that play a role in the synthesis and stabilization of CuQDs. A comparison of the FTIR spectra of the aqueous extract of pumpkin waste and the green-synthesized CuQDs showed distinct shifts and the presence of specific absorption bands, highlighting the involvement of various functional groups in the synthesis process. Overall, the CuQDs

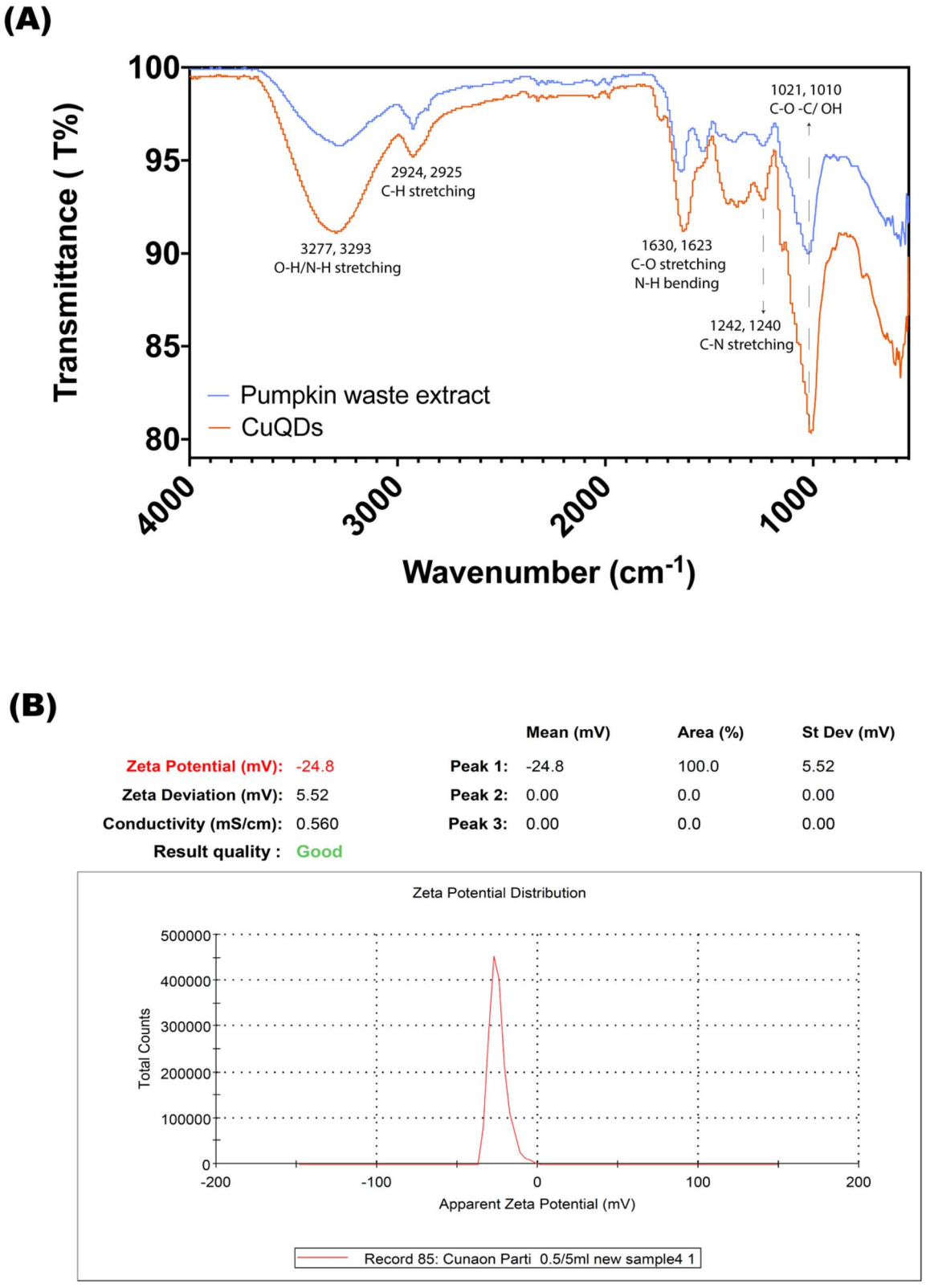

Fig. 3 (A): FTIR spectra of pumpkin waste extract and CuQDs. (B): The zeta potential analysis of the obtained CuQDs.

were functionalized with hydroxyl, carboxyl, carbonyl, and amino groups derived from organic moieties in the pumpkin waste extract. These groups endow the CuQDs with excellent water solubility, with no signs of aggregation.

3.1.5 Assessment of CuQDs stability. The CuQDs obtained from aqueous pumpkin waste extracts exhibited high stability. No sedimentation was found, and no significant changes in absorbance or fluorescence characteristics were observed.

Table 1 The FTIR spectra of the pumpkin waste and synthesized CuQDs showed the corresponding functional groups

Pumpkin frequencies (cm^{-1})	CuQDs frequencies (cm^{-1})	Functional group	Intensity	Assignment
3277.0	3293.0	O–H/N–H stretching	Strong	Alcohols, phenols, amines
2924.0	2925.0	C–H stretching	Variable	Aliphatic chains (phenols, flavonoids)
1630.0	1623.0	C=O stretching/N–H bending	Strong	Amide I (C=O) and amide II (N–H)
1532.0	—	C=C aromatic stretching	Variable	Aromatic rings (alkenes)
1380.0	1369.0	O–H bending/C–H aromatic	Variable	Polyphenols
1241.0	1240.0	C–N stretching	Variable	Aromatic amines
1021.0	1010.0	C–O–C stretching/–OH bending	Strong	Glycosidic bonds (carbohydrates)
650.0	604.0	C–H aromatic bending	Variable	Substituted aromatic compounds (flavonoids)
579.0	580.0	C–H out-of-plane bending	Variable	Alkanes

Furthermore, the stability was examined using the zeta potential. The zeta potential is a key parameter for determining QDs stability. A relatively high value indicates stronger repulsion between particles. This repulsion enhances stability over long storage times. The results of zeta potential measurements showed a value of −24.8 mV which depicts the high stability of the synthesized CuQDs (Fig. 3B). The stability of our pumpkin waste-derived CuQDs represents an advantage over conventional QDs and NPs. Our CuQDs exhibited potential for practical applications requiring extended shelf life.

QDs with zeta potential values greater than ±20 mV typically exhibit excellent stability due to strong electrostatic repulsion between particles. Our CuQDs exceed this threshold, demonstrating superior stability compared to many reported NPs.[29]

A recent study published in (2023) highlighted that QDs synthesized through green methods often exhibit enhanced stability compared to chemically synthesized counterparts due to the presence of natural stabilizing agents.[30] The authors noted that these CQDs retain high solubility, robust chemical inertness, facile modification, and good resistance to photobleaching, which aligns perfectly with our observations of pumpkin waste-derived CuQDs. Furthermore, the long-term stability of our CuQDs without additional stabilizers represents a significant economic advantage for large-scale applications. Developing an effective natural stabilizer or capping agent to prevent harmful components from leaching out of the QDs core makes economic sense for large-scale preparative goals.[19] Our approach achieves this through the natural biomolecules present in pumpkin waste, eliminating the need for expensive synthetic stabilizers. The significant stability of our pumpkin waste-derived CuQDs makes them suitable for such applications, offering advantages over less stable alternatives.

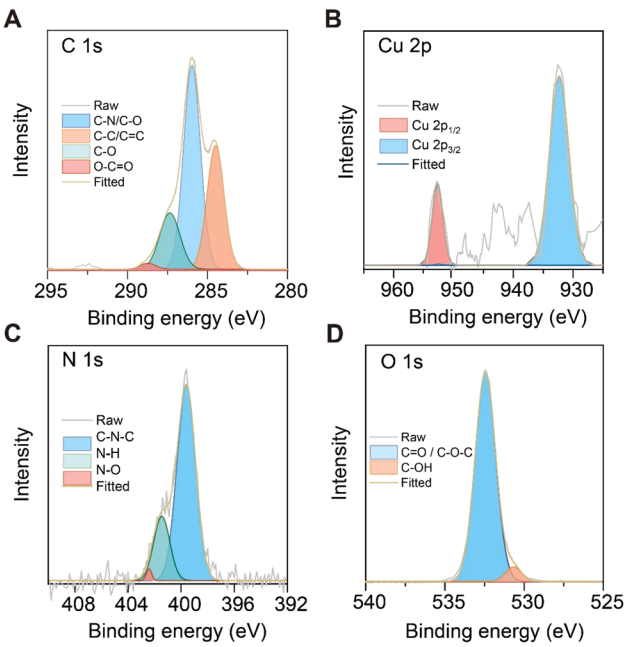

Fig. 4 High-resolution X-ray photoelectron spectroscopy (XPS) analysis of CuQDs: (A) C 1s, (B) Cu 2p, (C) N 1s and (D) O 1s spectra.

3.1.6 X-ray photoelectron spectroscopy (XPS) analysis. XPS was used to establish a potent surface-sensitive method for determining the chemical composition of the CuQDs. The peaks in the XPS wide-scan spectra for the green-synthesized CuQDs represent the presence of Cu, C, N, and O (Fig. 4). The peaks at 285.9, 399.6, 532.4, and 932.3 eV corresponded to C 1s, N 1s, O 1s, and Cu 2p, respectively. The high-resolution XPS spectrum of C 1s (Fig. 4A) was resolved into four peaks with binding energies of approximately 284.4, 285.9, 287.3, and 288.7 eV, corresponding to C–C/C=C, C– O/C–N, C–O, and O–C=O, respectively. The N 1s spectrum in Fig. 4C is fitted with three peaks at 399.6, 401.4, and 402.4 eV, which are ascribed to C–N–C, N–H, and N–O bonds, respectively. Deconvolution of the O 1s peak gives two components at 530.6, and 532.4 eV for the adsorbed oxygen, C–OH, and C–O–C/C=O (Fig. 4D), respectively, whereas fitting of the Cu 2p level spectrum in (Fig. 4B) represents two peaks located at 932.3 and 952.6 eV, corresponding to $2p_{3/2}$ and $2p_{1/2}$, respectively. The $2p_{3/2}$ binding energy of copper is commonly analyzed to obtain information about Cu-NPs and CuQDs surfaces, and the peak appeared at 932.3 eV confirmed the presence of Cu(0) and its oxidized state.[7] This peak is classically associated with the presence of Cu NPs and/or CuQDs.[31]

In the current experiment, two peaks were observed at 932.3 and 952.6 eV (Fig. 4B), which were assigned to the binding

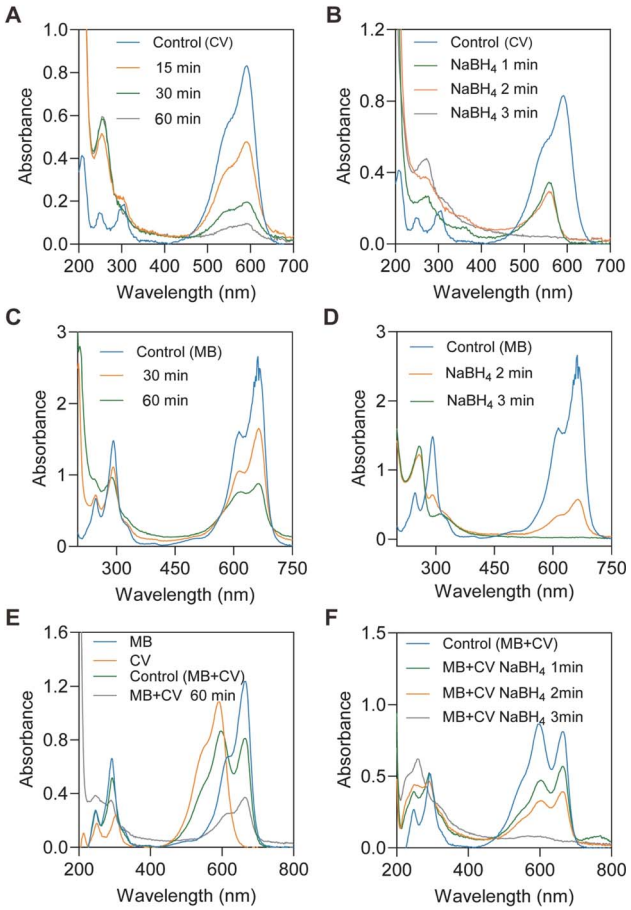

Fig. 5 UV-Vis spectra of (A) crystal violet reduction mediated by CuQDs at pH = 7 for 60 min. (B) Crystal violet (CV) reduction mediated by CuQDs and $NaBH_4$ for 3 min. (C) Methylene blue (MB) reduction by CuQDs at pH = 7 for 60 min. (D) Methylene blue (MB) reduction mediated by CuQDs and $NaBH_4$ for 3 min. (E) Crystal violet (CV) and methylene blue (MB) mixture reduction mediated by CuQDs at pH = 7 for 60 min. (F) Crystal violet (CV) and methylene blue (MB) mixture reduction mediated by CuQDs and $NaBH_4$ for 3 min.

energies of the $2p_{3/2}$ and $2p_{1/2}$ electrons of CuQDs/Cu(0), and no significant features for Cu(II) electrons were detected.[17]

The peaks at 530.6 eV and 532.4 eV for O 1s could indicate the presence of oxygen in the form of metal oxides (*e.g.*, Cu_2O) or hydroxyl/carbonyl groups from the green synthesis process. The peaks at 284.4 eV, 285.9 eV, 287.3 eV, and 288.7 eV for C 1s could indicate the presence of various carbon-containing groups (sp2 carbon, sp3 carbon, carbonyls, carboxyls, *etc.*) possibly derived from the organic precursors or capping agents used in the green synthesis method. The XPS results revealed that the surface of the oxygen-containing functionalized CuQDs was possibly associated with carbonyl and hydroxyl functional groups. Overall, these results were consistent with the FTIR analysis.

The combination of these peaks suggests that the CuQDs synthesized using the green method likely consist of metallic copper or copper oxide cores with surface functionalization involving organic molecules containing carbon, nitrogen, and oxygen functional groups. This surface functionalization can help stabilize QDs and impart additional properties derived from the green synthesis method.

3.2 Catalytic activity for dye degradation by green-synthesized CuQDs

The catalytic activity of the synthesized CuQDs in the reduction of CV, MB, and their mixtures was studied using UV-Vis spectroscopy. Fig. 5A and C show the reduction of CV and MB mediated by CuQDs at pH 7. Both spectra exhibit a gradual decrease in the characteristic absorbance peaks of CV (588 nm) and MB (664 nm) over time, indicating the degradation of both dyes by CuQDs under neutral pH conditions. As the time progressed from 15 to 60 min, the degradation became more pronounced, demonstrating the efficiency of CuQDs in reducing CV and MB.

In the case of the mixture of CV and MB (Fig. 5E and F), the reduction in CV appeared to be faster than that in MB. The absorbance peak corresponding to CV decreased more rapidly than that of MB, suggesting that CuQDs preferentially degrade CV over MB. This preferential degradation could be attributed to differences in dye structure, binding affinity to the CuQDs, or different reaction kinetics between the two dyes. Table 2 presents the corresponding degradation ratios of CV, MB, and their mixture, where CV showed a higher degradation (89.2%) than MB (60%) after 60 min, and the mixture showed a degradation of 79% for CV and 55% for MB. These findings suggest that CuQDs are effective in degrading both CV and MB, with a notable preference for CV, which could be beneficial in applications targeting the removal of more toxic dyes, such as CV, from polluted water sources.[7] The catalytic capabilities of our pumpkin waste-derived CuQDs demonstrate advantages over conventional methods for environmental remediation. Obtained CuQDs showed effective catalytic activity in the reduction of CV and MB dyes, with preferential degradation of CV (89.2%) over MB (60%) after 60 min, and significantly enhanced degradation rates in the presence of $NaBH_4$.

The preferential degradation of CV over MB by our CuQDs is particularly noteworthy, as it suggests potential selectivity in targeting specific pollutants. This selective catalytic activity has significant implications for wastewater treatment applications where certain dyes may be more toxic or persistent than others.

Table 2 Degradation ratios of CV, MB, and their mixtures under different conditions

Condition	Time consumed	Degradation ratio (%)
CV at pH 7 (without $NaBH_4$)	60 min	89.2%
CV with $NaBH_4$	3 min	95%
MB at pH 7 (without $NaBH_4$)	60 min	60%
MB with $NaBH_4$	3 min	90%
CV in mixture with $NaBH_4$	3 min	90%
MB in mixture with $NaBH_4$	3 min	96%
CV in mixture without $NaBH_4$	60 min	79%
MB in mixture without $NaBH_4$	60 min	55%

The preference for CV over MB degradation could be attributed to differences in molecular structure and interactions with the catalyst. CV is a triphenylmethane dye with a central carbenium carbon, which readily accepts electrons and hydrogen, facilitating a faster reduction to its leuco form. MB is a phenothiazine dye with a more stable heterocyclic structure, requiring more electrons for reduction and therefore degrading more slowly. Furthermore, the CuQDs surface is capped with phytochemical groups that impart negative charges. Cationic dyes adsorb strongly onto negatively charged surfaces.[32] CV has a higher positive charge density than MB, leading to stronger electrostatic attraction to the CuQDs. These factors combine to accelerate the degradation of CV compared with MB.

A recent study noted that green-synthesized QDs often exhibit enhanced catalytic activity due to their unique surface chemistry and high surface-to-volume ratio.[33] The authors highlighted that sustainable synthesis of QDs has several advantages such as the use of low-cost and non-toxic raw materials, simple operations, and environmentally friendly processes, which aligns perfectly with our approach using pumpkin waste.

The synergistic effect observed between our CuQDs and $NaBH_4$, resulting in dramatically accelerated degradation rates (CV: 95%, MB: 90% within 3 min), represents a significant advancement over conventional catalytic systems. This enhanced catalytic efficiency is particularly valuable for practical environmental applications where rapid dyes removal is essential. Furthermore, the formation of leucocrystal violet (LCV) (286 nm in UV-Vis) which is the reduced, colorless form of CV and less toxic derivative as reported by several studies.[34,35] These findings indicate that our CuQDs not only remove dyes but also transform them into less harmful compounds. This detoxification capability is particularly valuable compared to conventional adsorption-based methods that merely transfer pollutants from one phase to another without reducing their toxicity. A recent study emphasized that QDs synthesized through green methods often exhibit enhanced catalytic activity for environmental remediation applications.[20] The authors noted that CQDs synthesized through pyrolysis exhibit excellent biocompatibility, optical stability, and high QY, which contributes to their effectiveness in catalytic applications.

The effective dyes degradation achieved by our CuQDs without additional toxic chemicals represents an advantage over conventional methods that often rely on hazardous oxidizing agents. Our approach offers a sustainable alternative for wastewater treatment, utilizing agricultural waste to create effective catalysts for environmental remediation. This aligns with the growing emphasis on circular economy approaches in environmental technology, as highlighted in recent literature.[36]

3.3 Enhancement of catalytic activity by addition of $NaBH_4$

The catalytic degradation of CV and MB was significantly enhanced by the addition of $NaBH_4$. Fig. 5B and D show the reduction of CV and MB in the presence of $NaBH_4$. In both cases, the spectra show a rapid decrease in the absorbance peaks of CV and MB within 3 min after the addition of $NaBH_4$, indicating that the presence of $NaBH_4$ significantly accelerated the degradation process. The degradation of CV reached 95% within 3 min when $NaBH_4$ was added, compared to 89.2% in the absence of $NaBH_4$, and the degradation of MB increased from 60% to 90% in the same timeframe. A new absorption peak appeared at 286 nm during CV degradation, corresponding to the formation of LCV, a reduced and less toxic derivative of CV.[35] This transformation aligns with previous studies suggesting

Table 3 Comparison of the dye degradation performance of the CuQDs with other Cu-based catalysts

Catalyst	Dye and reductant/oxidant	Experimental conditions	Degradation efficiency and time	Reference
CuQDs	CV and MB with $NaBH_4$	100 μg mL^{-1} CuQDs; 0.5 mg mL^{-1} $NaBH_4$	Without $NaBH_4$: CV 89.2% and MB 60% after 60 min; with $NaBH_4$: CV 95% and MB 90% in 3 min	Present study
Biogenic Cu nanoflowers	MB with $NaBH_4$	MB + $NaBH_4$; CuNFs from *F. benghalensis* leaf extract	MB reduction increased to 72% in 85 min; negligible reduction without catalyst	Agarwal *et al.*, 2016 (ref. 39)
Redispersible CuO NPs	MB with H_2O_2	0.6 mM CuO; MB 53.5 μM; UV light; H_2O_2 at 0.5 or 1 mL	With H_2O_2 only: 53.3% MB reduction in 75 min; CuO + 0.5 mL H_2O_2: 87.4% MB reduction in 75 min; CuO + 1 mL H_2O_2: 99.6% MB degradation in 75 min	Wang *et al.*, 2025 (ref. 40)
CuO/PET nanocomposite	MB (photocatalytic)	10 ppm MB; UV lamp (10 W); 500 rpm stirring	MB removal 56.5% at 5 min and 77.5% at 10 min; 99% decolourisation within 30 min	Suhad *et al.*, 2021 (ref. 41)
CuO NPs with SDS surfactant	MB with $NaBH_4$	Precipitated CuO NPs modified with sodium dodecyl sulfate; $NaBH_4$ reductant	Total degradation of MB achieved in 10 min	Benhadria *et al.*, 2021 (ref. 42)

that LCV is less toxic than the parent dye and poses fewer environmental hazards.[37] In the mixture of CV and MB, the presence of $NaBH_4$ accelerated the degradation of both dyes (Fig. 5E and F). The degradation of CV and MB in the mixture was significantly faster in the presence of $NaBH_4$, with CV and MB showing degradation ratios of 90% and 96%, respectively, within 3 min. These results confirm that $NaBH_4$ enhances the degradation rate of both dyes, making the process much more efficient.

The results in Table 2 show the degradation ratios of CV, MB, and their mixture with $NaBH_4$. The addition of $NaBH_4$ to the system led to a substantial increase in the degradation rates, with CV and MB both degraded rapidly within 3 min. The degradation rates were 95% for CV and 90% for MB, compared to 89.2% and 60%, respectively, without $NaBH_4$. These results indicate that $NaBH_4$ plays a crucial role in enhancing the catalytic effect of CuQDs. $NaBH_4$ serves as an electron donor, transferring electrons to the dye molecules, which then interact with CuQDs, leading to their reduction and decolorization.[35] This synergistic effect between CuQDs and $NaBH_4$ enhances the catalytic efficiency, enabling faster dye degradation. These results support the potential use of CuQDs in environmental applications, particularly in wastewater treatment, where fast and efficient removal of toxic dyes is essential. The enhancement of catalytic activity by $NaBH_4$ further improves the viability of CuQDs for practical applications, ensuring faster and more efficient dyes removal.

The catalytic mechanism could be explained through a Langmuir–Hinshelwood model. In this model, both the dye molecules and the $NaBH_4$ reductant adsorb onto the surface of the CuQDs. BH_4^- ions donate electrons to the dye molecules, and the CuQDs act as electron relays.[38] This process lowers the activation barrier and converts the dye to its leuco form. The CuQDs remain unchanged after the reaction, functioning as true catalysts. The catalytic effect is enhanced in the presence of $NaBH_4$. Without $NaBH_4$, the degradation of CV and MB is slower. With $NaBH_4$, both dyes are reduced within min. BH_4^- acts as the electron donor, transferring electrons to the dye through the CuQDs. A schematic should illustrate this electron transfer process.

Table 3 compares the catalytic performance of the CuQDs with previously reported Cu-based catalysts. It lists the dye tested, the reaction conditions, the degradation efficiency, the time required, and the rate constants. This table shows that most Cu-based catalysts require tens of min to reduce MB or CV and often achieve lower degradation efficiency. By contrast, the current study's pumpkin-waste CuQDs, in combination with $NaBH_4$, achieve near-complete decolourisation of CV and MB within three min. Even without $NaBH_4$, the CuQDs remove 89.2% of CV and 60% of MB within 60 min. Thus, pumpkin-waste CuQDs catalyst displays faster and more efficient dye reduction than previously reported Cu materials.

Previous studies showed that CV undergoes catalytic degradation primarily through N-demethylation, followed by the destruction of its conjugated chromophore structure, ultimately leading to mineralization. The initial attack on the CV molecule often involves reactive species, such as hydroxyl radicals ($HO^{\bullet}$), generated in catalytic processes like Fenton-like reactions.[43] The degradation pathway typically proceeds *via* a series of N-demethylated intermediates. The sequential removal of methyl groups from the amino functionalities of CV results in compounds with progressively fewer methyl groups. These intermediates include, but are not limited to, *N*,*N*,*N*′,*N*′-tetramethyl-*p*-phenylenediamine, *N*,*N*,*N*′-trimethyl-*p*-phenylenediamine, *N*,*N*′-dimethyl-*p*-phenylenediamine, *N*-methyl-*p*-phenylenediamine, and eventually *p*-phenylenediamine. The loss of these methyl groups is a critical step in the decolorization process, as it disrupts the electron delocalization responsible for the dye's color.[43]

Further degradation involves the cleavage of the central carbon–nitrogen bonds and the opening of the aromatic rings. This can lead to the formation of smaller aromatic compounds, such as 4-(dimethylamino) benzophenone and 4,4′-bis (dimethylamino) benzophenone, before these are further oxidized and mineralized into simpler inorganic compounds like carbon dioxide (CO_2) and water (H_2O).[43,44] The efficiency of this mineralization depends heavily on the catalyst and reaction conditions employed.

MB also undergoes catalytic degradation through oxidative processes, typically initiated by reactive oxygen species. The degradation pathway for MB involves the cleavage of the thiazine ring, sequential demethylation, and subsequent opening of the aromatic rings, leading to its decolorization and eventual mineralization.[44]

The initial steps in MB degradation often involve the demethylation of the amino groups, similar to CV. This process yields several intermediate products, including Azure A, Azure B, Azure C, and thionin. These intermediates are less chromophoric than MB, contributing to the observed decolorization. The progressive removal of methyl groups weakens the chromophore structure, making the molecule more susceptible to further oxidative attack.[44]

Following demethylation, the central sulfur-containing thiazine ring is susceptible to cleavage. This ring opening, along with the subsequent oxidation of the aromatic rings, leads to the formation of smaller, non-toxic organic acids and aliphatic compounds. These smaller molecules are then further oxidized until complete mineralization to CO_2, H_2O, and inorganic ions such as sulfate and nitrate occurs.[44]

3.4 Antioxidant activity of CuQDs

In the present study, the DPPH antioxidant activity of the green-synthesized CuQDs was evaluated based on the free radical scavenging activity monitored by UV-Vis, where DPPH depicts the maximum absorption band at 517 nm because of its odd electron. DPPH is a stable free radical in which the color transformation occurs from violet to yellow as a result of reduction either through hydrogen or electron donation. In this process, the DPPH radical transforms into a stable diamagnetic compound, with the disappearance of the strong absorption band at 517 nm. The resulting de-colorization was stoichiometric with respect to the number of electrons taken up. Thus, substances that are capable of carrying out the aforementioned

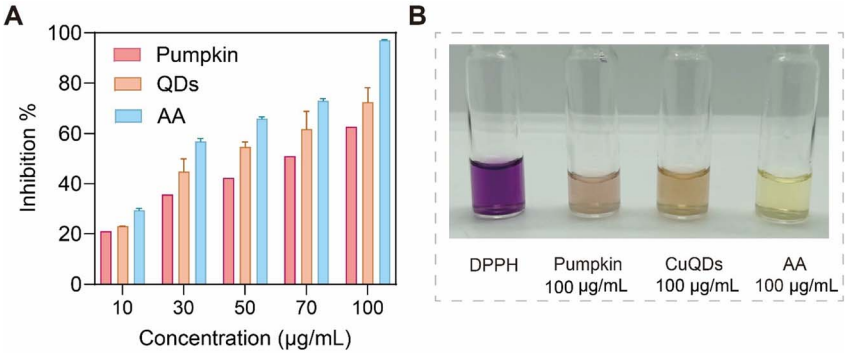

Fig. 6 The antioxidant effect of the green synthesized CuQDs. (A) The DPPH-based antioxidant activity of pumpkin waste extract, CuQDs, in addition to the Ascorbic acid which was used as a positive control. (B) Color modifications of DPPH in methanol mixture for pumpkin waste extract, CuQDs, and ascorbic acid at the same concentration after 30 min compared to the control DPPH color.

chemical reactions are known as antioxidants/radical scavengers.[45] Fig. 6A and B show the dose–response bar chart for the ratio of DPPH radical scavenging activity of the pumpkin waste extract alone and the CuQDs synthesis from pumpkin waste extract. It is clearly found that both pumpkin waste extract and CuQDs act as good antioxidants having inhibition activity in a dose-dependent manner. The CuQDs from pumpkin waste extract presented an effective antioxidant activity towards DPPH, with maximum free radical scavenging activity observed at 100 μg mL^{-1} of 79% within 30 min, which was better than that of pumpkin waste extract alone (69%). Moreover, the antioxidant activity of the CuQDs was compared with that of ascorbic acid (100 μg mL^{-1}), a strong antioxidant, as a positive control.

The enhanced antioxidant activity of CuQDs towards DPPH over pumpkin waste extract could be due to the greater oxidant being integrated on the surface of CuQDs owing to their greater surface-to-volume ratio.[7] Overall, the DPPH radical scavenging activity recorded for the CuQDs in the present study was due to the combined impact of CuQDs and polyphenolic compounds (from FTIR analysis) as capping and stabilizing agents. The DPPH scavenging activity of pumpkin waste-derived CuQDs (79% at 100 μg mL^{-1}) surpasses many reported Cu-based nanomaterials, such as Mangifera indica-synthesized CuQDs (72% at 100 μg mL^{-1})[9] and Eclipta alba-derived ZnO QDs (70%).[4] This performance is competitive, particularly given the eco-friendly synthesis route and the enhanced surface-to-volume ratio of CuQDs, which amplifies electron donation capacity compared to bulkier NPs or raw plant extracts (69% for pumpkin extract alone).

The enhanced antioxidant activity of our CuQDs compared to the pumpkin waste extract alone can be attributed to the quantum confinement effects and large surface area of the NPs. Our DPPH scavenging activity of 79% at 100 μg mL^{-1} surpasses many reported NPs in the literature, positioning our pumpkin waste-derived CuQDs as an effective antioxidant agent.[46] A comprehensive review by Moradialvand *et al.* (2025) emphasized that the surface chemistry of QDs significantly influences their biological activities, including antioxidant properties.[19] The authors noted that the surface functionalization of QDs, in addition to their composition, is crucial for the process of endocytosis and further reduces cytotoxicity, which aligns with our findings of enhanced biocompatibility and antioxidant activity.

Furthermore, the green synthesis approach enhances the biocompatibility of our CuQDs, making them particularly suitable for potential biomedical applications where both antioxidant activity and low toxicity are essential. A recently published article reported that QDs synthesized through green methods retain high solubility, robust chemical inertness, facile modification, and good resistance to photobleaching, which makes them ideal for various biomedical applications.[19] Our pumpkin waste-derived CuQDs align with these advantages, offering a sustainable and effective alternative to conventionally synthesized antioxidant agents.

3.5 Safety profile of CuQDs seed germination

Green gram (*Vigna radiata*) seeds were grown on Whatman filter paper with 6 seeds on Petri dishes soaked in CuQDs at a concentration of 0–100 μg mL^{-1} in order to examine the safety profile of green synthesis CuQDs on seed germination. CuQDs did not present any toxic effect on the used seeds; however, at 100 μg mL^{-1}, *Vigna radiata's* germination rate took longer for germination compared to the control group's seeds. In comparison to the untreated controls, seed germination and seedling growth were slightly slower at concentrations of 50, 80, and 100 μg mL^{-1} (Fig. 7A). Interestingly, seeds treated with low concentrations of CuQDs (10 and 30 μg mL^{-1}) showed rapid growth compared to the control and seeds treated with high concentrations of CuQDs (Fig. 7B). Therefore, the CuQDs displayed a safety profile comparable to that of biogenic copper NPs and copper oxide-based nanocarriers, as reported in earlier investigations.[47,48] Moreover, it may be inferred from these side-by-side observations that green-synthesized CuQDs are more secure for use in environmental applications. To ensure the reproducibility of the seed germination experiment, it was conducted three times under identical conditions. The data presented in the manuscript represent the average values from these three independent trials, confirming the reliability and consistency of the results observed.

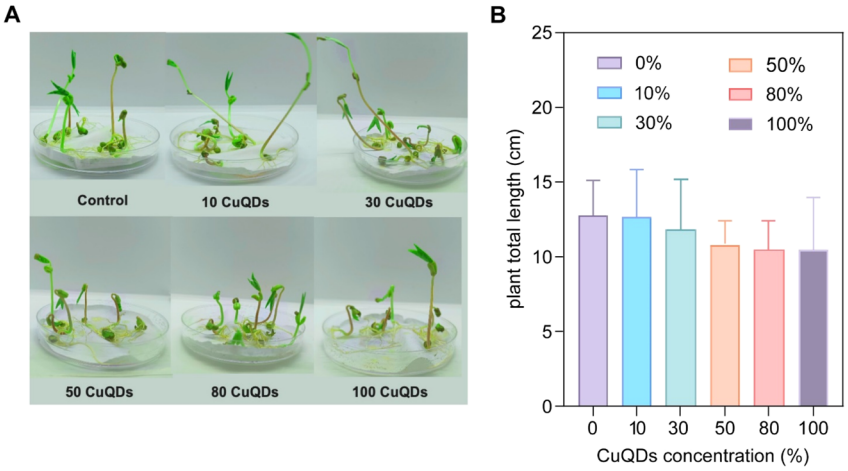

Fig. 7 Effect of CuQDs on germination of *Vigna radiata* seeds (A), and bar graph demonstrating the effects of CuQDs on seedling length after seven days (B).

3.6 Biocompatibility and safety evaluation

The biocompatibility and safety of the synthesized CuQDs were assessed using zebrafish embryos, following the OECD-203 protocol.[46,49] Zebrafish embryos were exposed to varying concentrations of CuQDs (0, 20, 40, 60, 80, and 100 μg mL^{-1}) for up to 120 hours post-fertilization (hpf). The embryos were observed under a light microscope to evaluate the development of key anatomical features, including the tail, head, and eye formation, as well as any potential deformities.

The biotoxicity of CuQDs was evaluated by exposing the zebrafish embryos to CuQDs concentrations ranging from 20 to 100 μg mL^{-1}, starting at 1.5 hpf. Observations at 24, 48, 72, and 96 hpf compared to untreated controls (Fig. 8A), 96 hpf showed no apparent phenotypic changes in the embryos exposed to

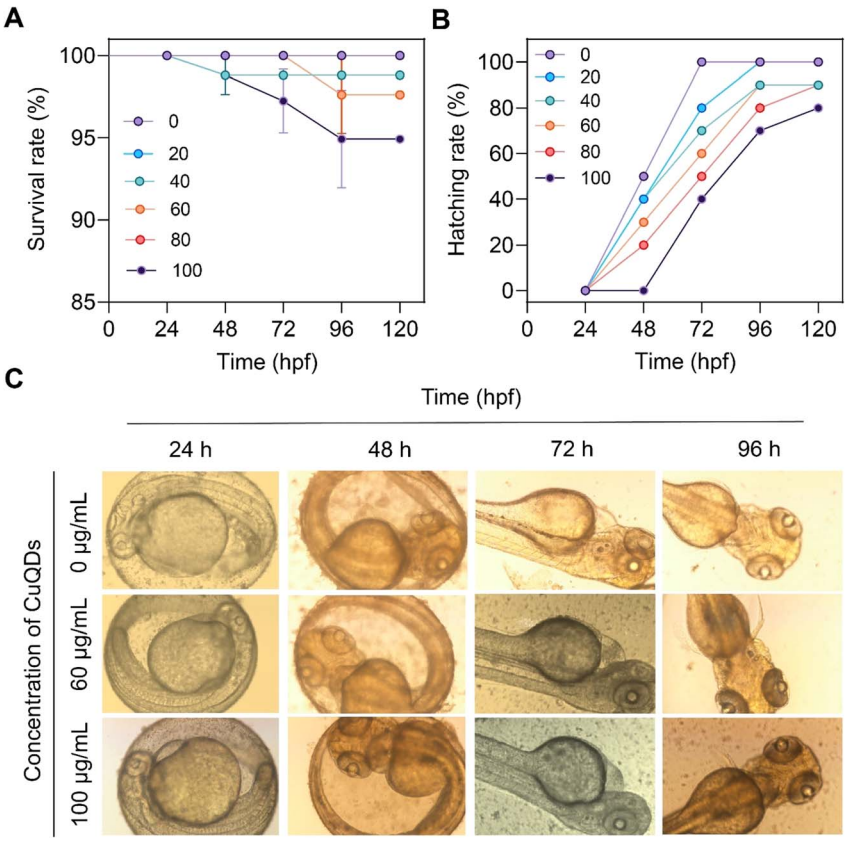

Fig. 8 Developmental and toxicity assessment of CuQDs in zebrafish embryos: (A) survival, (B) hatching rates, and (C) phenotypic observations at various concentrations.

CuQDs. The embryos developed normally across all concentrations, demonstrating the minimal toxicity of CuQDs, even at the highest concentration of 100 μg mL^{-1}. At 24 hpf, the hatching rates for the control (85%), 50 μg mL^{-1} CuQDs (80%), and 100 μg mL^{-1} CuQDs (75%) groups were observed. By 120 hpf, the hatching rates for the control (95%), 50 μg mL^{-1} CuQDs (90%), and 100 μg mL^{-1} CuQDs (85%) remained relatively unchanged (Fig. 8B). These results indicate that CuQDs exhibited minimal toxicity at all tested concentrations, with hatching success comparable between control and CuQDs-treated groups. Mortality rates were consistently below 4% across all CuQDs concentrations, underscoring negligible acute toxicity (Fig. 8C). Statistical analysis confirmed no significant differences in hatching or survival rates between the control and CuQDs-treated groups (P-value > 0.05), supporting the conclusion that CuQDs do not cause acute toxicity at concentrations up to 100 μg mL^{-1}.

Further validation of CuQDs' safety was conducted by assessing the development of key anatomical features such as the eyes, head, and tail. The normal development of these features, along with the successful hatching of the majority of embryos, further supports the biocompatibility of CuQDs. The absence of significant phenotypic changes and the normal development of embryos even at higher concentrations (100 μg mL^{-1}) strongly suggest that CuQDs do not induce major developmental disruptions. The slight delay in hatching observed at higher CuQDs concentrations is likely an adaptive response rather than a toxic effect, as embryos developed normally after hatching which aligns with documented adaptive responses to sub-lethal stressors, where organisms prioritize survival mechanisms over developmental timelines.[50] According to Moradialvand *et al.* (2025), toxicity concerns are a major limitation for many conventionally synthesized QDs, particularly those containing heavy metals.[19] The authors emphasize that addressing toxicity concerns is crucial for the safe use of QDs, highlighting the importance of developing biocompatible alternatives. Our pumpkin waste-derived CuQDs address this concern directly, demonstrating negligible toxicity even at higher concentrations, which positions them favorably for potential biomedical applications.

3.7 Bioimaging applications of CuQDs

Fluorescence bioimaging plays a pivotal role in visualizing biological processes at cellular and subcellular levels, offering high sensitivity and real-time monitoring capabilities.[13] QDs have emerged as promising candidates for bioimaging due to their favorable optical properties, including tunable fluorescence emission, high photostability, and low toxicity compared to traditional cadmium-based QDs.[13]

The bioimaging potential of CuQDs synthesized from pumpkin waste was evaluated using zebrafish embryos and larvae as *in vivo* models. Fluorescence imaging revealed robust tissue-specific accumulation of CuQDs, with bright fluorescence signals observed in the eyes, yolk sac, and intestinal tract. CuQDs entered the embryos *via* the germ ring and chorion through simple soaking. Given their small size, CuQDs were primarily deposited in the yolk sac (Fig. 9A). The fluorescence observed in the yolk sac is consistent with its role in nutrient processing during early developmental stages (Fig. 9B). Furthermore, intense fluorescence in the intestinal tract of zebrafish larvae highlighted the pathway of CuQDs absorption *via* swallowing, demonstrating their ability to selectively target metabolically active regions.

CuQDs demonstrated multicolor fluorescence properties under various excitation wavelengths. Upon exposure to UV light, CuQDs exhibited vivid blue fluorescence, while distinct emission colors were observed under blue and green filters, validating their excitation wavelength-dependent multicolor fluorescence properties. This versatility allows CuQDs to function as multicolor nano probes for real-time biological imaging. Merged fluorescence images further illustrated comprehensive tissue distribution and confirmed the uptake and transport pathways of CuQDs, including absorption through the yolk sac and skin, as well as selective targeting of ocular and digestive tissues (Fig. 9). These results highlight the suitability of pumpkin waste-derived CuQDs for bioimaging applications, emphasizing their strong fluorescence properties, tissue specificity, and safety profile.

The bioimaging potential of CuQDs synthesized from pumpkin waste was evaluated using zebrafish embryos and larvae as *in vivo* models. Fluorescence imaging revealed robust tissue-specific accumulation of CuQDs, with bright fluorescence signals observed in the eyes, yolk sac, and intestinal tract. CuQDs entered the embryos *via* the germ ring and chorion through simple soaking. Given their small size, CuQDs were primarily deposited in the yolk sac (Fig. 9A-a and B-a).

The fluorescence observed in the yolk sac is consistent with its role in nutrient processing during early developmental stages (Fig. 9A-a and B-a). For comparison with control groups in (Fig. 9A-b) Furthermore, intense fluorescence in the intestinal tract of zebrafish larvae highlighted the pathway of CuQDs absorption *via* swallowing, demonstrating their ability to selectively target metabolically active regions (Fig. 9B-c, and C-c).

CuQDs demonstrated multicolor fluorescence properties under various excitation wavelengths. Upon exposure to UV light, CuQDs exhibited vivid blue fluorescence, while distinct emission colors were observed under blue and green filters, validating their excitation wavelength-dependent multicolor fluorescence properties. This versatility allows CuQDs to function as multicolor nano probes for real-time biological imaging. Merged fluorescence panels in Fig. 9 further illustrate comprehensive tissue distribution and confirm uptake and transport pathways *via* yolk sac, skin, and digestive tract.

Collectively, Fig. 9B, and C visualizes the differential fluorescence intensities between CuQDs-exposed and control groups across developmental time points and tissues, supporting the selective and biocompatible nature of CuQDs *in vivo*. These results highlight the suitability of pumpkin waste-derived CuQDs for bioimaging applications, emphasizing their strong fluorescence properties, tissue specificity, and safety profile.

CuQDs also demonstrated multicolor emission under different excitation sources. Blue, green, and red channels each revealed distinct signals, and merged images highlighted comprehensive distribution across tissues. This excitation-dependent fluorescence validates their potential as multicolor

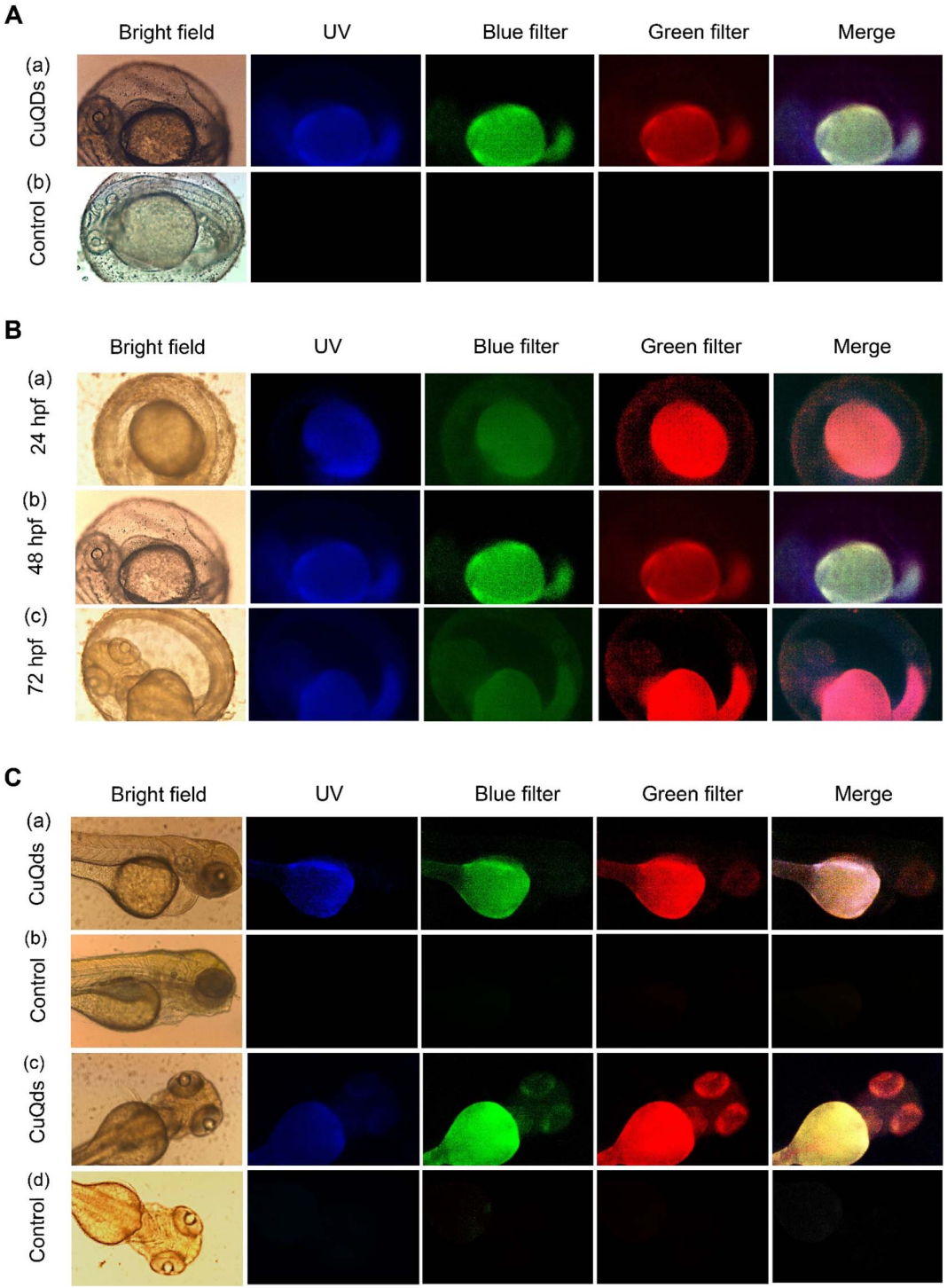

Fig. 9 Fluorescence imaging of CuQDs distribution in zebrafish embryos and larvae: tissue-specific accumulation and multicolor emission under different excitation wavelengths. Panel A compares CuQDs-treated embryos with untreated controls. Under UV, blue, and green filters, embryos exposed to CuQDs displayed bright fluorescence in the yolk sac, while controls showed no signal. Panel B shows stage-dependent distribution at 24, 48, and 72 hpf. At all stages, embryos retained strong yolk sac fluorescence. The intensity and distribution broadened over time, with clear localization in metabolically active tissues, including the intestinal tract. Panel C illustrates larvae at later stages. CuQDs-treated larvae exhibited intense fluorescence in the eyes, yolk sac, and intestinal tract. These signals confirm uptake through both ingestion and tissue absorption. Controls again showed no detectable emission.

probes for real-time *in vivo* imaging. Together, Fig. 9 demonstrates that CuQDs selectively accumulate in key tissues, are readily visualized across developmental stages, and remain biocompatible. Their strong and tunable fluorescence properties highlight their suitability for diagnostic and biomedical imaging applications.

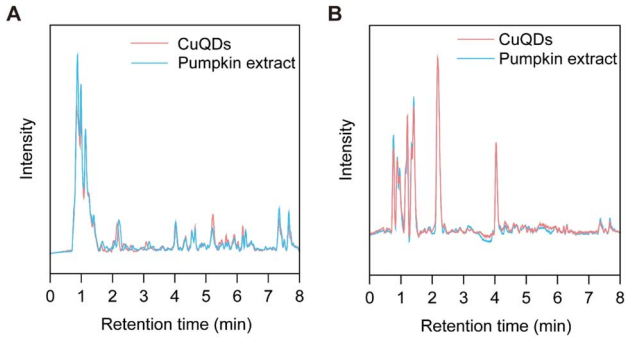

Fig. 10 LC–MS total ion chromatograms (TICs) of pumpkin waste and copper quantum dots (CuQDs) synthesized using the pumpkin waste extract. (A) Negative ionization mode and (B) positive ionization mode.

3.8 Phytochemical-driven mechanism of CuQDs green synthesis

LC-MS analysis in both negative and positive ionization modes revealed significant chemical transformations during the green synthesis of CuQDs. Fig. 10 shows representative total ion chromatograms (TICs) of pumpkin extract and CuQDs in negative mode (A) and positive mode (B). Tables 4 and 5 summarize the key compounds identified in negative and positive modes, respectively, along with their percent changes after CuQDs synthesis. Compounds were classified based on their roles in the synthesis process.

The LC-MS analysis of CuQDs synthesis using pumpkin extract reveals a comprehensive three-phase mechanism, providing novel insights into the roles of specific phytochemicals throughout the process. Based on the data, the green synthesis mechanism involves distinct chemical transformations that can be categorized into reduction, nucleation/growth, and stabilization phases. During the reduction phase, several compounds showed significant decreases or complete disappearance, indicating their role as reducing agents. The primary reduction reactions involve phenolic acid-mediated reduction, where R–OH represents phenolic compounds such as chlorogenic acid and caffeic acid; flavonoid-mediated reduction, where Fl–$(OH)_2$ represents flavonoids with catechol or pyrogallol B-rings; and nitrogen compound-mediated reduction, where R–NH_2 represents amino acids, phenolic amines, and alkaloids. This multi-component reduction system demonstrates that pumpkin extract functions through synergistic pathways. Phenolic acids with catechol moieties showed complete consumption, consistent with their strong reducing capabilities due to electron-rich hydroxyl groups. The hierarchical pattern of consumption suggests a sequential reduction process where compounds with the strongest reducing power initiate Cu^{2+} reduction, followed by contributions from moderate reducing agents. Positive mode analysis revealed the significant contribution of nitrogen-containing compounds (amino acid derivatives, −72.10%; phenolic amines, −56.98%) to the reduction process, a finding underreported in previous green synthesis studies.[51] This synergistic reduction involving both oxygen and nitrogen-containing functional groups likely enhances the efficiency and control of QDs formation.

Following reduction, the nucleation and growth phase begins as Cu^0 atoms aggregate to form nuclei, which then grow into QDs. Compounds showing minimal changes, such as cucurbitacins (−2.70%), may serve as templates or scaffolds for QDs formation. This templating effect may contribute to the controlled formation of QDs with specific morphologies. The appearance of new compounds such as shikimic acid and nucleosides indicates biomolecule fragmentation during the redox process, potentially establishing a dynamic equilibrium that influences growth kinetics. In the final stabilization/capping phase, several compounds showed significant increases or appeared as new peaks, indicating their role as capping agents. One of the most significant findings is the identification of a multi-layer capping mechanism involving primarily lipophilic compounds. The dramatic increases in fatty acid derivatives (+639.07%), tocopherols (+322.92%), and triterpenes (+104.39%) suggest these compounds form a primary hydrophobic layer around the QDs. This is complemented by a secondary layer of flavonoid derivatives and vitamin-mediated surface passivation, explaining the high stability of green-synthesized CuQDs.[52] This multi-layer model advances beyond

Table 4 Key compounds identified in negative mode and their changes during CuQDs synthesis

RT (min)	Tentative compound	Area change (%)	Role in synthesis
0.88	Organic acids (*e.g.*, citric acid)	−9.02	Minor reducing agent
1.14	Quinic acid	−39.05	Significant reducing agent
2.22	Chlorogenic acid	−100.00	Critical reducing agent
2.43	Caffeic acid	−100.00	Critical reducing agent
2.65	*p*-Coumaric acid	−100.00	Critical reducing agent
3.00	Ferulic acid	−100.00	Critical reducing agent
3.18	Sinapic acid	−77.12	Primary reducing agent
3.63	Flavonoid glycoside	−68.45	Primary reducing agent
4.93	Flavonoid aglycone	−78.51	Primary reducing agent
2.07	Chlorogenic acid isomer	+140.08	Reaction product/stabilizer
3.81	Flavonoid glycoside	+64.15	Capping agent
4.55	Kaempferol derivative	+57.59	Capping agent
1.24	Shikimic acid	New	Reaction product
2.92	Ferulic acid derivative	New	Reaction product

Table 5 Key compounds identified in positive mode and their changes during CuQDs synthesis

RT (min)	Tentative compound	Area change (%)	Role in synthesis
0.98	Organic acids (protonated)	−31.51	Significant reducing agent
1.34	Choline derivatives	−31.77	Significant reducing agent
1.63	Alkaloids (minor)	−100.00	Critical reducing agent
1.76	Phenolic amines	−56.98	Primary reducing agent
1.92	Amino acid derivatives	−72.10	Primary reducing agent
3.15	Apigenin derivatives	−65.93	Primary reducing agent
3.23	Luteolin derivatives	−36.25	Significant reducing agent
2.18	Cucurbitacins	−2.70	Template/scaffold
1.19	Vitamin B derivatives	+53.29	Reaction product/stabilizer
4.04	Sterol derivatives	+30.35	Capping agent
4.33	Triterpenes	+104.39	Primary capping agent
4.51	Fatty acid derivatives	+639.07	Primary capping agent
4.60	Tocopherols (vitamin E)	+322.92	Primary capping agent
1.05	Nucleosides	New	Reaction product
4.88	Phytosterols	New	Primary capping agent

the conventional focus on polyphenols as primary capping agents and explains the high colloidal stability often observed in plant extract-synthesized NPs.[53] The arrangement of lipophilic tails toward the QDs surface with polar head groups extending outward provides both steric and electrostatic stabilization. Clear structure-activity relationships emerged from the analysis. Among phenolic compounds, those with higher numbers of hydroxyl groups showed greater decreases, supporting the hypothesis that reducing power correlates with hydroxylation patterns. For flavonoids, aglycone forms exhibited greater reducing capability than glycosides, likely due to the absence of sterically hindering glycosidic moieties. The detailed understanding of this three-phase mechanism has important implications for controlled synthesis of CuQDs. By identifying specific compounds involved in each phase, these findings enable rational optimization of synthesis conditions.

The presence of tocopherols and phytosterols in the capping layer suggests these CuQDs may possess inherent antioxidant properties beneficial for biomedical applications.[54] Furthermore, this study demonstrates the value of waste valorization in nanotechnology, showing that pumpkin waste can serve as an effective source of both reducing and capping agents for high-value QDs, contributing to sustainable chemistry principles. The process involves the three stages: activation, growth, and stabilization. In the activation stage, copper ions (Cu^{2+}) are reduced to zero-valent copper (Cu^{0}) by bio-reducing agents, such as polyphenols and flavonoids present in pumpkin waste extracts. These compounds, with their hydroxyl (-OH) groups, donate electrons, reducing Cu^{2+} to Cu^{0}. In the growth stage,

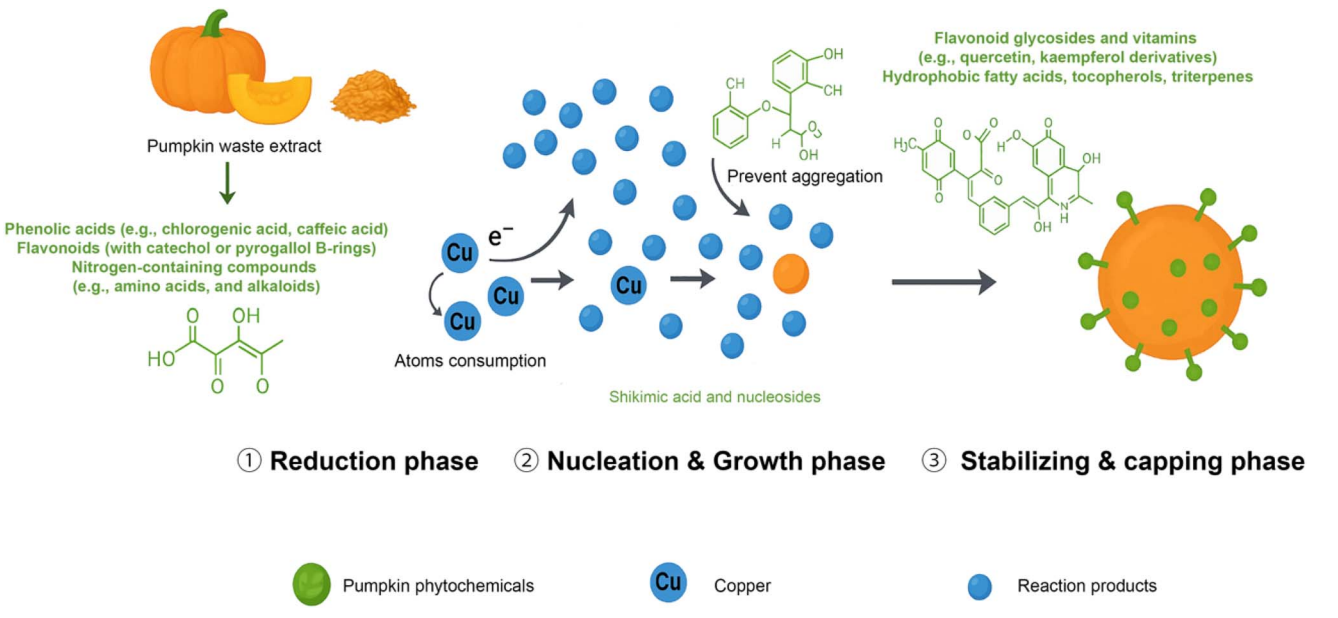

Fig. 11 1Schematic diagram illustrating the three-phase mechanism. This visual representation aids in comprehending the process discussed in the manuscript.

small Cu^0 atoms spontaneously aggregate into NPs with enhanced thermodynamic stability. The stabilization stage results in the formation of spherical CuQDs, which achieve the most energetically favorable conformation. The three-phase mechanism is visually summarized in Fig. 11, which enhances the understanding of the process.

This approach consistent with green chemistry principles, offering a sustainable and efficient synthesis of CuQDs. This method eliminates the need for toxic chemicals and expensive synthetic stabilizers, presenting an advantage over conventional synthesis techniques. The synthesis of QDs has several benefits, such as the use of low-cost, non-toxic materials, simple operations, and environmentally friendly processes.[33] The natural reduction of copper ions using pumpkin waste extracts avoids the need for harsh chemical agents, while the growth and stabilization stages occur spontaneously without the need for controlled conditions or additional stabilizers. These features demonstrate the cost-effectiveness and eco-friendliness of this approach.[29]

4. Conclusion

Our study developed CuQDs from pumpkin waste *via* a three-phase, phytochemical-driven synthesis. Mechanistic investigations *via* LC-MS revealed the underlying processes of reduction, nucleation, and stabilization during CuQDs formation. The process produced monodisperse dots with strong fluorescence. In dye reduction experiments, CuQDs alone removed 89.2% of CV and 60% of MB within 60 min. Adding $NaBH_4$ accelerated the reaction; CV and MB removal reached 95% and 90% within three min. The dots also exhibited antioxidant capacity, achieving 79% DPPH radical scavenging at 100 μg mL^{-1} within 30 min. Biocompatibility assessments showed no morphological defects in zebrafish embryos; hatching rates remained between 85% and 95%, and mortality stayed below 4% up to 100 μg mL^{-1}. Seed germination assays found that low concentrations (10–30 μg mL^{-1}) promoted growth, whereas higher doses slightly delayed germination. Collectively, these findings confirm that pumpkin-derived CuQDs function as efficient catalysts, potent antioxidants and safe bioimaging probes. Future work should focus on scaling up this green synthesis and testing the CuQDs in real wastewater treatment. Evaluating long-term biodistribution and clearance *in vivo* will be essential for biomedical translation. Screening other agricultural wastes as precursors could yield QDs with tailored properties. These directions could expand the environmental and biomedical applications of this sustainable nanomaterial. Future studies could delve deeper into the precise chemical structures of dye degradation products using advanced analytical techniques like GC-MS and ion chromatography. Additionally, further insights into the photophysical properties of these CuQDs, such as their fluorescence lifetime, would be valuable but were beyond the scope of this current experimental capabilities in this study.

Declarations

All experiments were performed in compliance with the relevant laws and institutional guidelines.

Author contributions

Lamis Dayoub: Investigation, methodology, formal analysis, writing – original draft, software, data curation. Xiaoxuan Li: Validation, writing – review & editing, methodology, data curation. Shoulei Yan: Methodology, software, data curation, writing – review & editing. Xuewen Peng: Investigation, validation, software. Wajeeha Pervaiz: Writing – review & editing. Yiping Chen: Conceptualization, resources, supervision, writing – review & editing, funding acquisition, project administration.

Conflicts of interest

The authors declare that they have no competing financial interests or personal relationships that could have appeared to influence the work reported in this paper.

Abbreviations

CuQDs	Copper quantum dots
CV	Crystal violet
MB	Methylene blue
QDs	Quantum dots
FTIR	Fourier transform infrared spectroscopy
TEM	Transmission Electron Microscopy
HRTEM	High-resolution transmission electron microscopy
SAED	Selected area electron diffraction
XPS	X-ray photoelectron spectroscopy
LC-MS	Liquid chromatography–mass spectrometry
DPPH	1,1-Diphenyl-2-picrylhydrazyl
$NaBH_4$	Sodium borohydride
GRAS	Generally recognized as safe
UV-Vis	Ultraviolet-visible spectroscopy
HPLC	High-performance liquid chromatography
RT (min)	Retention time (minutes)
hpf	Hours post-fertilization
dpf	Days post-fertilization
QY	Quantum yield
TIC	Total ion chromatogram
V. radiata	*Vigna radiata*

Data availability

The data that support the findings of this study are available from the corresponding author upon reasonable request.

Acknowledgements

The authors thank the National Natural Science Foundation of China (32172293) and Liaoning Province "Xingliao Talent Plan" Leading Talent Project (XLYC2402036) for financial support.

References

1 A. Hussain, T. Kausar, A. Din, M. A. Murtaza, M. A. Jamil, S. Noreen, H. u. Rehman, H. Shabbir and M. A. Ramzan,

Determination of total phenolic, flavonoid, carotenoid, and mineral contents in peel, flesh, and seeds of pumpkin (Cucurbita maxima), *J. Food Process. Preserv.*, 2021, **45**, e15542.

2 N. H. A. Kadir, N. Murugan, A. A. Khan, A. Sandrasegaran, A. U. Khan and M. Alam, Evaluation of the cytotoxicity, antioxidant activity, and molecular docking of biogenic zinc oxide nanoparticles derived from pumpkin seeds, *Microsc. Res. Tech.*, 2024, **87**, 602–615.

3 A. Marzban, S. Z. Mirzaei, M. Karkhane, S. K. Ghotekar and A. Danesh, Biogenesis of copper nanoparticles assisted with seaweed polysaccharide with antibacterial and antibiofilm properties against methicillin-resistant Staphylococcus aureus, *J. Drug Deliv. Sci. Technol.*, 2022, **74**, 103499.

4 A. K. Singh, P. Pal, V. Gupta, T. P. Yadav, V. Gupta and S. P. Singh, Green synthesis, characterization and antimicrobial activity of zinc oxide quantum dots using Eclipta alba, *Mater. Chem. Phys.*, 2018, **203**, 40–48.

5 S. Momeni, R. Ahmadi, A. Safavi and I. Nabipour, Blue-emitting copper nanoparticles as a fluorescent probe for detection of cyanide ions, *Talanta*, 2017, **175**, 514–521.

6 J. Li and N. Wu, Semiconductor-based photocatalysts and photoelectrochemical cells for solar fuel generation: a review, *Catal. Sci. Technol.*, 2015, **5**, 1360–1384.

7 H. Rani, S. P. Singh, T. P. Yadav, M. S. Khan, M. I. Ansari and A. K. Singh, In-vitro catalytic, antimicrobial and antioxidant activities of bioengineered copper quantum dots using Mangifera indica (L.) leaf extract, *Mater. Chem. Phys.*, 2020, **239**, 122052.

8 A. Llorens, E. Lloret, P. A. Picouet, R. Trbojevich and A. Fernandez, Metallic-based micro and nanocomposites in food contact materials and active food packaging, *Trends Food Sci. Technol.*, 2012, **24**, 19–29.

9 S. Behera, L. Shubhadarshinee, P. Mohapatra, B. R. Jali, P. Mohapatra and A. K. Barick, Green Synthesis, Characterization, and Acoustical Analysis of Copper Quantum Dots (Cu QDs) Using Leaf Extract of Mangifera indica Plant, *J Mol Eng Mater*, 2023, **11**, 2350001.

10 Y. Lv, L. Zhang, R. Wu and L. S. Li, Recent progress on eco-friendly quantum dots for bioimaging and diagnostics, *Nano Res.*, 2024, **17**, 10309–10331.

11 S. Paulraj, K. Raman, C. R. Mohan, J. Ramachandiran, K. Ashokkumar and M. Pambayan Ulagan, Biosynthesis of Eudrilus eugeniae vermi wash based enzyme decorated copper oxide nanoparticles towards seed germination of green gram, *J Agric Food Res*, 2022, **9**, 100343.

12 R. Mariselvam, A. Ranjitsingh, C. Padmalatha and P. M. Selvakumar, Green synthesis of copper quantum dots using Rubia cardifolia plant root extracts and its antibacterial properties, *J Acad Ind Res*, 2014, **3**, 191–194.

13 N. Abu, S. Chinnathambi, M. Kumar, F. Etezadi, N. M. Bakhori, Z. A. Zubir, S. N. M. Salleh, R. H. Shueb, S. Karthikeyan and V. Thangavel, Development of biomass waste-based carbon quantum dots and their potential application as non-toxic bioimaging agents, *RSC Adv.*, 2023, **13**, 28230–28249.

14 U. J. Pyati, A. T. Look and M. Hammerschmidt, Zebrafish as a powerful vertebrate model system for *in vivo* studies of cell death, *Semin. Cancer Biol.*, 2007, **17**, 154–165.

15 Q. Wan, Y. Song, Z. Li, X. Gao and H. Ma, In vivo monitoring of hydrogen sulfide using a cresyl violet-based ratiometric fluorescence probe, *Chem. Commun.*, 2013, **49**, 502–504.

16 M. A. A. Orabi, M. M. Salem-Bekhit, E. I. Taha, E.-S. Abdel-Sattar, O. S. Alqahtani, F. A. Al-Joufi, B. A. Abdel-Wahab, A. M. Alshabi, H. S. Alyami, J. Ahmad and T. Hatano, Design, Characterization, and Antimicrobial Evaluation of Copper Nanoparticles Utilizing Tamarixinin a Ellagitannin from Galls of Tamarix aphylla, *Pharmaceuticals*, 2022, **15**, 216.

17 W. Wei, Y. Lu, W. Chen and S. Chen, One-Pot Synthesis, Photoluminescence, and Electrocatalytic Properties of Subnanometer-Sized Copper Clusters, *J. Am. Chem. Soc.*, 2011, **133**, 2060–2063.

18 A. Sachdev and P. Gopinath, Green synthesis of multifunctional carbon dots from coriander leaves and their potential application as antioxidants, sensors and bioimaging agents, *Analyst*, 2015, **140**, 4260–4269.

19 Z. Moradialvand, L. Parseghian and H. R. Rajabi, Green synthesis of quantum dots: Synthetic methods, applications, and toxicity, *J. Hazard. Mater. Adv.*, 2025, **18**, 100697.

20 P. K. Praseetha, R. I. J. Litany, H. M. Alharbi, A. A. Khojah, S. Akash, M. Bourhia, A. A. Mengistie and G. A. Shazly, Green synthesis of highly fluorescent carbon quantum dots from almond resin for advanced theranostics in biomedical applications, *Sci. Rep.*, 2024, **14**, 24435.

21 Q. Sun, X. Sun, H. Dong, Q. Zhang and L. Dong, Copper quantum dots on TiO2: A high-performance, low-cost, and nontoxic photovoltaic material, *J. Renewable Sustainable Energy*, 2013, **5**, 021413.

22 N. U. M. Nizam, M. M. Hanafiah, E. Mahmoudi and A. W. Mohammad, Synthesis of highly fluorescent carbon quantum dots from rubber seed shells for the adsorption and photocatalytic degradation of dyes, *Sci. Rep.*, 2023, **13**, 12777.

23 T. P. M. Daby, U. Modi, A. K. Yadav, D. Bhatia and R. Solanki, Bioimaging and therapeutic applications of multifunctional carbon quantum dots: Recent progress and challenges, *Next Nanotechn*, 2025, **8**, 100158.

24 M. Najaflu, M. Shahgolzari, F. Bani and A. Y. Khosroushahi, Green Synthesis of Near-Infrared Copper-Doped Carbon Dots from Alcea for Cancer Photothermal Therapy, *ACS Omega*, 2022, **7**, 34573–34582.

25 P. Huang, X. Liu, X. Liu, J. Wei, F. Liu and H. Li, One-pot synthesis of Cu:InP multishell quantum dots for near-infrared light-emitting devices, *Nano Res.*, 2024, **17**, 10655–10660.

26 P. Pandya, T. J. Webster and S. Ghosh, Nanobioprospecting of photoautotrophs for the fabrication of quantum dots: mechanism and applications, *Front. Chem*, 2024, **12**, 1458804.

27 P. Punniyakotti, P. Panneerselvam, D. Perumal, R. Aruliah and S. Angaiah, Anti-bacterial and anti-biofilm properties

of green synthesized copper nanoparticles from Cardiospermum halicacabum leaf extract, *Bioprocess Biosyst. Eng.*, 2020, **43**, 1649–1657.

28 T. Boobalan, M. Sethupathi, N. Sengottuvelan, P. Kumar, P. Balaji, B. Gulyás, P. Padmanabhan, S. T. Selvan and A. Arun, Mushroom-Derived Carbon Dots for Toxic Metal Ion Detection and as Antibacterial and Anticancer Agents, *ACS Appl. Nano Mater.*, 2020, **3**, 5910–5919.

29 H. H. Jing, F. Bardakci, S. Akgöl, K. Kusat, M. Adnan, M. J. Alam, R. Gupta, S. Sahreen, Y. Chen, S. C. B. Gopinath and S. Sasidharan, Green Carbon Dots: Synthesis, Characterization, Properties and Biomedical Applications, *J Funct Biomater*, 2023, **14**, 27.

30 K. Anpalagan, J. V. Karakkat, R. Jelinek, N. N. Kadamannil, T. Zhang, I. Cole, K. Nurgali, H. Yin and D. T. H. Lai, A Green Synthesis Route to Derive Carbon Quantum Dots for Bioimaging Cancer Cells, *Nanomaterials*, 2023, **13**, 2103.

31 E. Benassai, M. Del Bubba, C. Ancillotti, I. Colzi, C. Gonnelli, N. Calisi, M. C. Salvatici, E. Casalone and S. Ristori, Green and cost-effective synthesis of copper nanoparticles by extracts of non-edible and waste plant materials from Vaccinium species: Characterization and antimicrobial activity, *Mater. Sci. Eng. C*, 2021, **119**, 111453.

32 A. Haleem, A. Shafiq, S. Q. Chen and M. Nazar, A Comprehensive Review on Adsorption, Photocatalytic and Chemical Degradation of Dyes and Nitro-Compounds over Different Kinds of Porous and Composite Materials, *Molecules*, 2023, **28**, 1081.

33 S. Iravani and R. S. Varma, Green synthesis, biomedical and biotechnological applications of carbon and graphene quantum dots. A review, *Environ. Chem. Lett.*, 2020, **18**, 703–727.

34 M. Sengan, D. Veeramuthu and A. Veerappan, Photosynthesis of silver nanoparticles using Durio zibethinus aqueous extract and its application in catalytic reduction of nitroaromatics, degradation of hazardous dyes and selective colorimetric sensing of mercury ions, *Mater. Res. Bull.*, 2018, **100**, 386–393.

35 H. Kolya and C.-W. Kang, Biogenic Synthesis of Silver-Iron Oxide Nanoparticles Using Kulekhara Leaves Extract for Removing Crystal Violet and Malachite Green Dyes from Water, *Sustainability*, 2022, **14**, 15800.

36 J. Shang, Q. Zhou, K. Wang and Y. Wei, Engineering of Green Carbon Dots for Biomedical and Biotechnological Applications, *Molecules*, 2024, **29**, 4508.

37 A. M. Abdelfatah, M. Fawzy, A. S. Eltaweil and M. E. El-Khouly, Green Synthesis of Nano-Zero-Valent Iron Using Ricinus Communis Seeds Extract: Characterization and Application in the Treatment of Methylene Blue-Polluted Water, *ACS Omega*, 2021, **6**, 25397–25411.

38 S. M. Padre, S. Kiruthika, S. Mundinamani, S. Ravikirana, S. Surabhi, J. R. Jeong, K. M. Eshwarappa, M. S. Murari, V. Shetty, M. Ballal and C. G. S, Mono- and Bimetallic Nanoparticles for Catalytic Degradation of Hazardous Organic Dyes and Antibacterial Applications, *ACS Omega*, 2022, **7**, 35023–35034.

39 M. Agarwal, A. Singh Bhadwal, N. Kumar, A. Shrivastav, B. Raj Shrivastav, M. Pratap Singh, F. Zafar and R. Mani Tripathi, Catalytic degradation of methylene blue by biosynthesised copper nanoflowers using F. benghalensis leaf extract, *IET Nanobiotechnol*, 2016, **10**, 321–325.

40 Q. Wang, G. Gao, D. Gong and C. Zhang, Redispersible CuO nanoparticles: preparation and photocatalytic capacity for the degradation of methylene blue, *RSC Adv.*, 2025, **15**, 19023–19033.

41 S. A. Yasin, S. Y. Sharaf Zeebaree, A. Y. Sharaf Zeebaree, O. I. Haji Zebari and I. A. Saeed, The Efficient Removal of Methylene Blue Dye Using CuO/PET Nanocomposite in Aqueous Solutions, *Catalysts*, 2021, **11**, 241.

42 N. Benhadria, M. Hachemaoui, F. Zaoui, A. Mokhtar, S. Boukreris, T. Attar, L. Belarbi and B. Boukoussa, Catalytic Reduction of Methylene Blue Dye by Copper Oxide Nanoparticles, *J. Cluster Sci.*, 2022, **33**, 249–260.

43 L. Wang, C. Zhou, Y. Yuan, Y. Jin, Y. Liu, Z. Jiang, X. Li, J. Dai, Y. Zhang, A. A. Siyal, W. Ao, J. Fu and J. Qu, Catalytic degradation of crystal violet and methyl orange in heterogeneous Fenton-like processes, *Chemosphere*, 2023, **344**, 140406.

44 Y. S. Jara, T. T. Mekiso and A. P. Washe, Highly efficient catalytic degradation of organic dyes using iron nanoparticles synthesized with Vernonia Amygdalina leaf extract, *Sci. Rep.*, 2024, **14**, 6997.

45 P. R. Prasad, S. Kanchi and E. B. Naidoo, In-vitro evaluation of copper nanoparticles cytotoxicity on prostate cancer cell lines and their antioxidant, sensing and catalytic activity: One-pot green approach, *J. Photochem. Photobiol. B: Biol.*, 2016, **161**, 375–382.

46 S. Ali, K. G. Sudha, N. Thirumalaivasan, M. Ahamed, S. Pandiaraj, V. D. Rajeswari, Y. Vinayagam, M. Thiruvengadam and R. Govindasamy, Green Synthesis of Magnesium Oxide Nanoparticles by Using Abrus precatorius Bark Extract and Their Photocatalytic, Antioxidant, Antibacterial, and Cytotoxicity Activities, *Bioengineering*, 2023, **10**, 302.

47 M. I. Nabila and K. Kannabiran, Biosynthesis, characterization and antibacterial activity of copper oxide nanoparticles (CuO NPs) from actinomycetes, *Biocatal Agric Biotechnol*, 2018, **15**, 56–62.

48 M. Alavi, S. Dehestaniathar, S. Mohammadi, A. Maleki and N. Karimi, Antibacterial Activities of Phytofabricated ZnO and CuO NPs by Mentha pulegium Leaf/Flower Mixture Extract against Antibiotic Resistant Bacteria, *Adv Pharm Bull*, 2021, **11**, 497–504.

49 ATT. Fish, *OECD Guideline for Testing of Chemicals*, 2000, vol. 1, p. 16.

50 P. A. Anila, J. Sutha, D. Nataraj and M. Ramesh, In vivo evaluation of Nano-palladium toxicity on larval stages and adult of zebrafish (Danio rerio), *Sci. Total Environ.*, 2021, **765**, 144268.

51 M. K. Hameed, I. M. Ahmady, C. Han and A. A. Mohamed, Efficient synthesis of amino acids capped gold nanoparticles from easily reducible aryldiazonium

tetrachloroaurate(III) salts for cellular uptake study, *Amino Acids*, 2020, **52**, 941–953.

52 P. Sharma, S. Kumari, D. Ghosh, V. Yadav, A. Vij, P. Rawat, S. Kumar, C. Sinha, S. Saini, V. Sharma, M. I. Hassan, C. M. Srivastava and S. Majumder, Capping agent-induced variation of physicochemical and biological properties of α-Fe2O3 nanoparticles, *Mater. Chem. Phys.*, 2021, **258**, 123899.

53 A. K. Sidhu, N. Verma and P. Kaushal, Role of biogenic capping agents in the synthesis of metallic nanoparticles and evaluation of their therapeutic potential, *Front Nanotechnol*, 2022, **3**, 801620.

54 A. M. Salazar-Bryam, I. Yoshimura, L. P. Santos, C. C. Moura, C. C. Santos, V. L. Silva, R. B. Lovaglio, R. F. Costa Marques, M. Jafelicci Junior and J. Contiero, Silver nanoparticles stabilized by ramnolipids: Effect of pH, *Colloids Surf., B*, 2021, **205**, 111883.